# Monolithic single longitudinal mode Nd-laser using a volume Bragg grating

**Ida Häggström**



Master of Science Thesis

Laser Physics
Department of Applied Physics
School of Engineering Science
KTH

Stockholm, Sweden 2006

TRITA-FYS: 2006-80
ISSN: 0280-316X
ISRN: KTH/FYS/–06:80-SE

**Abstract**

In this master thesis project a monolithic, single longitudinal mode laser cavity was designed and constructed. The laser output was frequency-locked by the use of a volume Bragg grating. Two gain media were proposed, Nd:glass and Nd:$GdVO_4$. The glass was found inadequate for this project due to it's poor thermal properties, leading to only $GdVO_4$ being used. The cavity components were attached by PDMS rubber, forming a compact, monolithic cavity of optical length 6.4 mm. The resulting laser output was operating in single longitudinal mode with a bandwidth of $< 360$ MHz with a stability of $< 66$ MHz over 10 s, attained using a Fabry-Pérot interferometer. The maximum laser power in $TEM_{00}$ mode was 30 mW for 2.1 W pumping, with a 1.5% power fluctuation. Temperature adjustment of the cavity allowed continous tuning of the laser frequency corresponding to an interval of 84 GHz (0.32 nm).

**Sammanfattning**

I detta examensarbete designades och konstruerades en monolitisk laserkavitet som opererade i en enda longitudinell mod. Två laserförstärkarmaterial studerades, Nd:glas och Nd:$GdVO_4$. Glaset visade sig vara otillräckligt för detta projekt på grund av sina dåliga termiska egenskaper, varvid endast Nd:$GdVO_4$ användes. Kavitetskomponenterna sammanfogades med hjälp av PDMS-gummi för att bilda en kompakt, monolitisk kavitet av optisk längd 6.4 mm. Lasern opererade i en enda longitudinell mod med bandbredd $< 360$ MHz och en stabilitet på $< 66$ MHz över 10 s, uppmätt med en Fabry-Pérot-interferometer. Den maximala lasereffekten i en $TEM_{00}$-mod var 30 mW för pumpeffekten 2.1 W, med en effektfluktuation på 1.5%. Temperaturändring av kaviteten tillät en kontinuerlig frekvensjustering av lasern motsvarande ett intervall på 84 GHz (0.32 nm).

**Acknowledgements**

First and foremost I would like to thank my adviser Björn Jacobsson for his invaluable support, practically guiding me in the lab as well as advising me theoretically. Without his expertise, my work would have been most difficult, not to say impossible. In addition, I'm highly grateful to my examiner Fredrik Laurell for allowing me to conduct this project within his research group, and throughout the experiments constantly hatching new ideas of approach. Furthermore, I would like to thank my office partners, especially Patrik, for putting up with my endless questions. Finally, I would like to express my gratitude to all the people in the Laserphysics research group for always taking time to help me in the lab or trying to find solutions for my questions. The time I spent with all of you has been a great experience, workwise of course, but not least for all the good times we've spent together in the lunch room, on the football field or "after work". Thank you all!

# Contents

# 1 Introduction

The idea of manipulating light in order to create a laser was already born in the early 20th century by Albert Einstein and his A and B coefficients, using the discoveries of Max Planck. The theory evolved and within some decades the first laser was built in the late 50's-early 60's [2]. Ever since, the laser theory has been widely expanded and a vast number of practical applications have been found.

In this day and time, devices (mainly electrical, but also optical) are shrinking in size to form more compact and efficient appliances. One such idea is the *monolithic* laser cavity; *a solid state lasers where the whole laser cavity consists only of one piece of crystal or glass* [1]. Straying slightly from the strict definition, it also allows several materials, bound together to form a single unit. The aim of this master thesis was to construct such a laser, using neodymium as the lasing material, thus producing an IR laser at roughly 1.06 $\mu$m. Furthermore, a volume Bragg grating was to be added to the setup in order to frequency-lock the laser output.

The work was carried out at KTH, the Royal Institute of Technology, Stockholm, courtesy of the Laserphysics research group.

## 1.1 Laser design

There were some restrictions associated with the design; single longitudinal mode operation, and if possible also single transverse mode operation to create a high quality laser output. The reason for single longitudinal mode operation being a stable, frequency-locked output, not switching between several longitudinal modes. Moreover, a monolithic setup is usually more stable than an ordinary laser since all components are assembled and their relative alignment is fixed.

Furthermore, to create this single longitudinal mode operation, a volume Bragg grating was to be used as a cavity mirror. Having a very narrow reflection band, the use of such device within the cavity will suppress other modes aside from the one at the reflection peak to lase, resulting in the Bragg grating working as a filter.

For simplicity one could coat the gain medium directly to let it act as the other cavity mirror. For a monolithic device however, the degrees of freedom when aligning the cavity are limited. Instead, a curved lens, coated to act as a mirror, was added to the setup. This allows alignment of both the curved mirror as well as the flat Bragg grating by translation and rotation of the cavity respectively. Moreover, to attach all cavity components to each other, silicone rubber (PDMS) was used as glue due to it's excellent optical properties as well as being an easy material to work with when attaching the components.

In reality, not only one but two monolithic setups were constructed, one

using Nd:glass as gain medium and the other one using Nd:$GdVO_4$. The selection of $GdVO_4$ was based on it's quite good emission peak overlap with the Bragg grating reflectivity peak at 1066 nm. In addition, the use of a Nd doped glass gain material is fairly unexplored in this type of setup. The benefits would be plenty for a working setup (see section 3.2.1.1), why also this material was to be studied.

Before managing building a working setup as the one described above, simpler setups were built as stepping stones towards the monolithic cavity.

## 1.2 Applications

The applications for a monolithic laser are many. They can be used for basically any purpose as the "normal" solid state lasers, with (most likely) the exception of high power lasers. The applications include medicine, telecommunications, measurement technique, sensors, non-linear frequency conversion and so on. Since the laser will also be narrowbanded, it can be useful for many types of measurements including spectroscopy. Furthermore, having very small dimensions, the laser can be used in smaller devices demanding a more compact component. In addition, demands of more stable setups may be fulfilled by a monolithic laser.

## 1.3 Objective

The objective for this thesis was construction of a monolithic laser setup, producing a single longitudinal mode output, by the use of a volume Bragg grating. The possibility to use either Nd:glass or Nd:$GdVO_4$ as gain medium was investigated, by studying some of the material properties and by conducting some relevant experiments. Further investigation of the laser output produced by the monolithic cavity was carried out, such as determination of the beam quality ($M^2$), pumping threshold and laser bandwidth. Other interesting properties like the possibility of frequency tunability was also looked into.

## 1.4 Outline

The outline of this thesis is as follows: In chapter 2 some of the measurement techniques used are presented, as well as some related theory. Section 3 will present the material used for the setups, focusing on the two gain media Nd:glass and Nd:$GdVO_4$. In the following section 4 it is investigated whether or not it is possible to build a working setup using Nd:glass, by using a working setup made with Nd:$YVO_4$. The two following sections 5 and 6 are stepping stones towards a monolithic setup, built in order to learn alignment and check lasing thresholds. Section 7 describes a monolithic setup and presents the most important results. The last setup is described in section 8, where the setup in the previous section is flipped and one component is

switched, yielding new results. The last section concludes the thesis work and some suggestions for future work are presented.

# 2 Measurement techniques

The beam quality is a property of great importance when constructing a laser with other purposes than e.g. only high output power. Usually the quality is determined by the *beam propagation factor*, also known as $M^2$. In order to understand this factor, one has to know something about gaussian beams. Furthermore, the highest resolution of the spectrum analyzers used was 0.07 nm. Any quantity (such as bandwidth, mode separation and frequency shift) smaller than this value will be unresolved. To be able to get more accurate values, a Fabry-Pérot interferomter was used. All experiments were conducted in laboratories provided by the Laserphysics research group at Albanova, KTH.

## 2.1 Gaussian beams

The simplest form of laser beam has an intensity distribution following a gaussian profile depicted in Fig.2.1. It is hence referred to as a *gaussian beam*. The radius of the beam is denoted $w$ and is defined as the distance from the peak intensity to the point where the intensity has dropped to $1/e^2$ of the maxiumum value. $2w$ is called the *beam waist*. The gaussian profile is

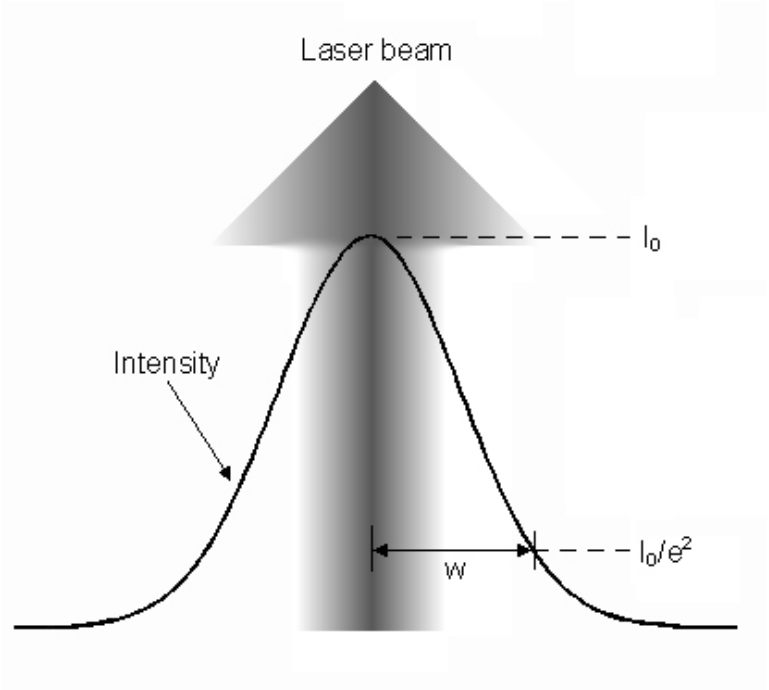


***Figure 2.1.*** *Description of a gaussian beam. The intensity distribution is gaussian, and the beam has a radius w.*

also known as the fundamental transverse mode, or $TEM_{00}$. In some cases however, there are higher order transverse modes present, causing a change in the intensity distribution. The analytical expression for the intensity distribution in the $xy$-plane for a beam can be derived into [4]

$$I_{mn}(x,y) = H_m(\frac{\sqrt{2}x}{w})H_n(\frac{\sqrt{2}y}{w})e^{-(x^2+y^2)/w^2}, \tag{2.1}$$

where $m$ and $n$ determine the order of the mode. The $H_i$ are the *Hermite polynomials* denoted [4]

$$H_i(u) = (-1)^i e^{u^2}\frac{d^i(e^{-u^2})}{du^i}. \tag{2.2}$$

The fundamental mode is thus expressed by Eq.2.1 for $m = n = 0$, yielding $I_{00}(x,y) = TEM_{00} = e^{-(x^2+y^2)/w^2}$ which is the gaussian distribution function mentioned earlier. The next transverse mode profiles are called $TEM_{01}$, $TEM_{10}$, $TEM_{02}$ and so forth. Some of the higher crossection beam profiles are seen in Fig.2.2 [2].

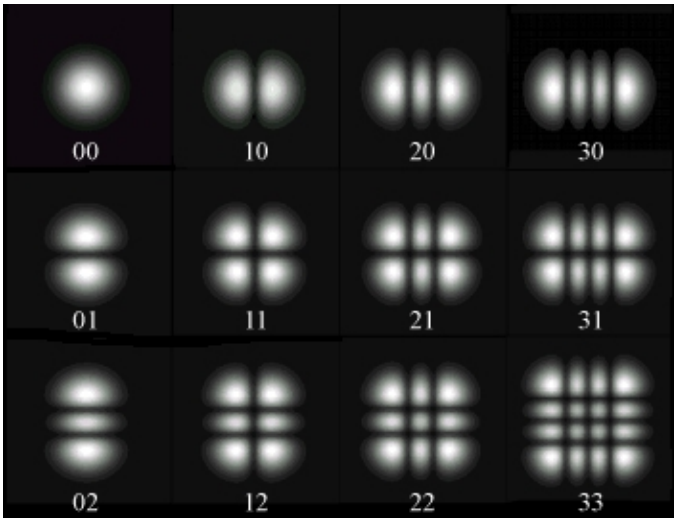


***Figure 2.2.*** *Fundamental transverse mode pattern $TEM_{00}$, followed by higher order TEM modes [2].*

### 2.1.1 Beam propagation factor $M^2$

In order to determine beam quality, the *beam propagation factor* $M^2$ is defined. It is a measure of how much a real laser beam deviates from a pure gaussian shape. The highest quality beam is gaussian with an $M^2$ value of 1. Inside the laser cavity, the beam will have a narrowest point, called the

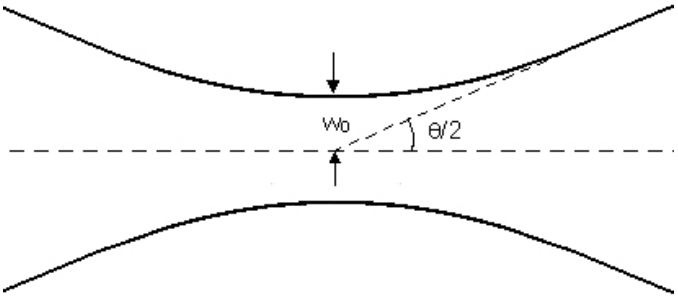


***Figure 2.3.*** *Definition of the beam waist $w_0$ for a gaussian laser beam. The beam divergence angle is $\theta/2$.*

*beam waist* depicted in Fig.2.3. For a purely gaussian beam, the beam has a waist $w_0$ and is diverging with an angle $\theta/2$ (total divergence $\theta$). For a real laser beam however, the minimum waist $W_0$ and angle $\Theta$ are defined as [4]

$$W_0 = w_0 M, \tag{2.3}$$

$$\Theta = \theta M. \tag{2.4}$$

The product of the total divergence angle and the beam waist of a gaussian beam is always the constant $2\lambda/\pi$. This relation is still valid for real beams, using the real angle and waist from Eq.2.3 and 2.4, yielding [4]

$$W_0 \Theta = M^2 \frac{2\lambda}{\pi}. \tag{2.5}$$

Using the above relation, the beam propagation factor can be determined by measuring the beam waist and divergence angle.

#### 2.1.1.1 The knife-edge technique

The technique most often used to determine $M^2$ is the knife-edge technique. A view of the setup is seen in Fig.2.4. The laser beam is focused by a lens to produce a new beam waist W'$_0$ and the total divergence angle $\Theta'$. The total power of the beam is then measured using a power meter. Then, a knife-edge (a razor in this case) is placed in the focus, partly blocking the beam. Integrating the gaussian function $e^{-2r^2/w^2}$ from $r = -w/2..w/2$ yields 68% of the total integral ($r = -\infty..\infty$), leaving 16% on either side. Thus, the distance between the two points where 82% and 16% of the total power is passing respectively corresponds to $2 \cdot w/2$ equal to the the beam radius W'$_0$. Similarly, the far field (at a distance far away from the beam waist) divergence angle $\Theta'/2$ is found by measuring the beam waist at a few

different far field points, and calculating the angle between them. By the use of Eq.2.5, $M^2$ can be calculated.

Sometimes it is interesting to know the beam waist within the cavity. Unfortunately, this quantity is usually hard or impossible to measure using a knife-edge since the cavity components are in the way or the beam waist is located within the gain medium. However, Eq.2.5 can be used, solving for $W_0$. Knowing $M^2$, and calculating the divergence angle $\Theta$ using the same method as for $\Theta'$, the cavity beam waist $W_0$ can be found.

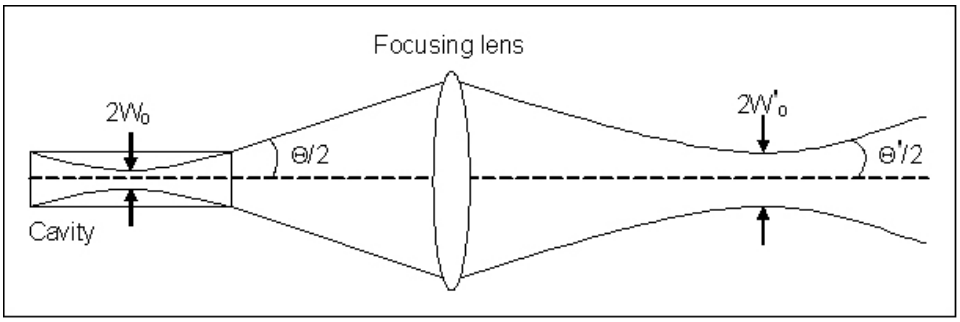


***Figure 2.4.*** *Scematic wiew of the setup for measuring $M^2$. The diverging angles are the far field angles.*

## 2.2 Fabry-Pérot interferometer

A Fabry-Pérot interferometer is a device consisting of two adjustable, parallel mirrors. A light ray incident upon the interferometer will thus bounce back and forth between the mirrors, each bounce resulting in a loss corresponding to the mirror transmission or reflection depending on what ray is considered. If assumed that light of amplitude $E_0$ is incident upon the first mirror, then the case for two mirrors of equal reflectance $R=r^2$ and transmittance $T=t^2$ is seen in Fig.2.5(a). As usual, R+T=1. To see the full derivation in this section, see reference [4] which has supplied the following theory. The reflections in Fig.2.5 will of course go on forever, even though only a few rays are depicted in the figure. If the electric field has an angle of incidence $\theta$ and the interferometer has length $L$ as shown in Fig.2.5(b), the extra path length traveled by one of two successive transmitted rays (exiting the second mirror) is

$$a + b = 2Lcos\theta. \tag{2.6}$$

Under the assumption of normal incidence $\theta = 0$ the path difference will simply be $2L$. If further assumed that the electric field is a plane wave, it propagates according to $e^{ikz}$ where $k = 2\pi/\lambda$ is the wave vector and $z$ is the path of propagation, in this case $z = 2L$. The phase factor $\phi$ of the wave is

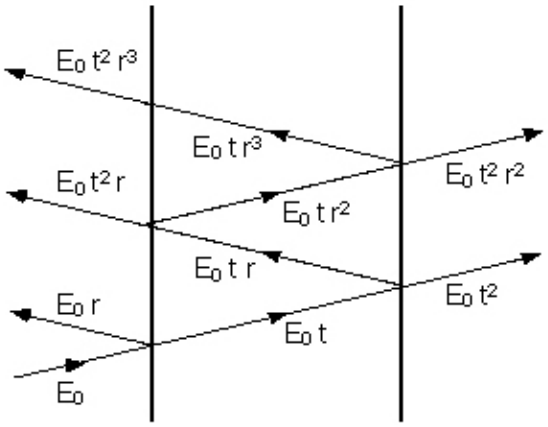


***(a)*** *Electric field amplitude undergoing multiple reflections from the two mirrors.*

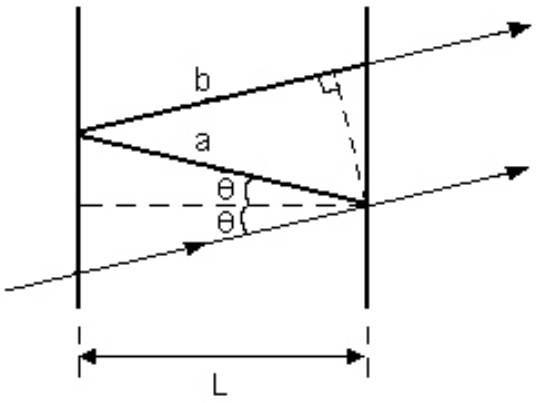


***(b)*** *Path difference for two successive transmissions*

***Figure 2.5.*** *Interferometer reflections.*

denoted as the real part of the exponent, thus equal to $kz$. Consequently,

$$\phi = k2L = \frac{4\pi}{\lambda}L. \tag{2.7}$$

Each electric field amplitude transmitted through the second mirror will contribute to the total total transmitted amplitude $E_t$ so that

$$E_t = E_0t^2 + E_0t^2r^2 + ... \tag{2.8}$$

After some derivation, it is found that Eq.2.8 is simply a geometric series, leading to the simplified result

$$E_t = E_0 \frac{T}{1 - Re^{i\phi}} \Longrightarrow I_t = I_0 \frac{T^2}{|1 - Re^{i\phi}|^2}, \tag{2.9}$$

where $I_t$ is the transmitted intensity using $I_t = |E_t|^2$. If discarding that the wave undergoes a phase change upon reflection, then further derivations give the relation

$$\frac{I_t}{I_0} = \frac{1}{1 - F' sin^2(\phi/2)}, \tag{2.10}$$

for $F' = 4R/(1-R)^2$. The above function is known as the *Airy function*. It is noted that $I_t/I_0$ reaches maximum values when $\sin(\phi/2) = 0$ or $\phi/2 = m\pi$ for m=0,1,2... . Apparently, the intensity will have an infinite series of peaks for the different phases $\phi$, as seen in Fig.2.6. Using $\phi$ from Eq.2.7 gives the relation

$$2m\pi = \frac{4\pi}{\lambda} L. \tag{2.11}$$

This yields the wavelengths $\lambda_{max,m}$ corresponding to the maximum intensity output of the interferometer

$$\lambda_{max,m} = \frac{2L}{m} \Longrightarrow \nu_{max,m} = \frac{mc}{2\eta L}. \tag{2.12}$$

The frequency separation between two maxima, $\Delta\nu$ can thus be found to be

$$\Delta\nu = \nu_{max,m+1} - \nu_{max,m} = \frac{c}{2\eta L}[(m+1) - m] = \frac{c}{2\eta L}. \tag{2.13}$$

### 2.2.1 Longitudinal mode separation

A laser cavity is designed so that a certain wavelength will oscillate within it. The cavity length is determined based on standing waves. The cavity length will hence be an even number of half the lasing wavelength. However, there are many wavelengths that will fulfill the standing wave criteria as well, hence will be able to oscillate in the cavity too. A laser cavity is thus a Fabry-Pérot resonator with a gain medium, since it is simply light bouncing between two mirrors, where at least one is partly transmitting. Thus, the longitudinal cavity modes can be leveled with the Fabry-Pérot modes. It was just shown that the frequency separation between these modes, i.e. mode separation $\Delta\nu$, can be derived into

$$\Delta\nu = \frac{c}{2\eta L}, \tag{2.14}$$

where $c = 3 \cdot 10^8$ m/s$^2$ [3] is the speed of light in vacuum, $\eta$ is the refractive index of the cavity medium and $L$ is the cavity length. In most cases

however, the cavity doesn't consist of only one medium. Taking this into consideration, $\eta L$ can be rewritten as $\sum_i \eta_i L_i$ where $\eta$ and $L$ are the same as before but connected to the medium indexed $i$. The sum is referred to as the *optical path length*. The number of modes able to oscillate within the cavity is limited by the gain bandwidth of the gain medium. Due to *spatial hole burning* there may be more than one longitudinal mode able to oscillate, since there is unused gain where the nodes are located for the fundamental standing wave (the first longitudinal mode). However, if there is a filter present in the cavity which has a very narrow reflection band, such as the outcoupler or incoupler, this might be the limiting factor of the number of modes instead [11].

If one instead wants to study the mode separation $\Delta\lambda$ expressed in wavelength $\lambda$, it is possible to use the relation $\Delta\nu = (-)c\Delta\lambda/\lambda^2$ in 2.14 to get

$$\Delta\lambda = \frac{\lambda^2}{2\sum_i \eta_i L_i}. \tag{2.15}$$

#### 2.2.1.1 Single longitudinal mode criterion

When building a setup, the output beam quality has to be considered. For this project, single longitudinal mode oscillation is desired. This criterion restrict cavity length. In order to get only one longitudinal mode in the laser output, the reflectance bandwidth of the in/outcoupler can be used. For the setups described in sections 6,7 and 8, the reflectance bandwidth of the Bragg grating is the limiting factor of the number of oscillating modes. It is found that the grating reflection has a full width half maximum, FWHM, of about 0.2 nm. Thus, if the cavity is designed so that the longitudinal mode separation is larger than this value, only one single mode should be able to oscillate. Using equation 2.15, the cavity length yielding single mode oscillation for a given setup can be found. In this case, the maximum optical path length is about $3mm$. If one allows the mode separation to be slightly smaller, the cavity can be a bit longer. For the monolithic setups described later on, the optical cavity length will be around 6.4 mm, still able to produce single mode output. For further reading on the possibility for single mode operation using a longer cavity, see reference [11].

### 2.2.2 Finesse

When discussing a Fabry-Pérot interferomter, it is important to mention it's $finesse$ F. It can is in one way be thought of as a measure of the device resolution. The finesse $F$ is defined as [2]

$$F = \frac{\Delta\nu}{\delta\nu} = \frac{\pi\sqrt{R}}{1-R}, \tag{2.16}$$

where $\Delta\nu$ is the mode separation and $\delta\nu$ is the full width half maximum (FWHM) of the peak seen in Fig.2.6. $R = r^2$ is still the reflectance. Obviously, for a fixed mode separation, a larger finesse yields a smaller FWHM and thus a better resolution.

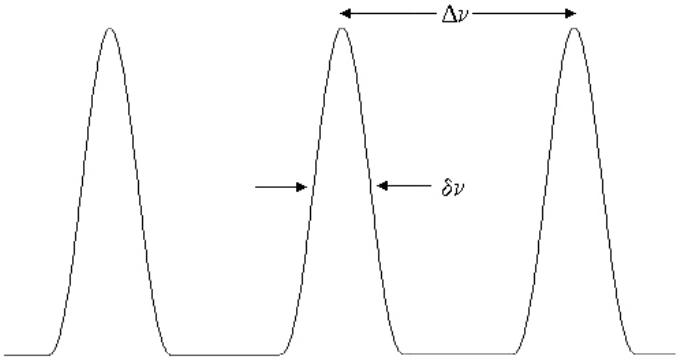


***Figure 2.6.*** *Modeseparation $\Delta\nu$ and FWHM $\delta\nu$ on a train of peaks.*

## 2.3 Fabry-Pérot setup

A Fabry-Pérot scanning interferomter by Tec-Optics was used to determine mode separation and laser temperature dependence in this project. As discussed above, the intensity within such interferometer will be a train of peaks, each peak with a different phase order $m$. Hence, the interferometer output will be a train of such peaks, multiplied with the emission peak of the laser resulting in another train of peaks. Their separation is determined by Eq.2.13. Since the separation is given as the distance between two successive maxima, any maxima can be used (any $m$, $m+1$). The result is that the interferometer output will only give a relative frequency for the peaks, and not the actual mode frequency. Hence, all results (plots) attained by the Fabry-Pérot will only show the frequency separation and not the real value of the frequency. The output will simply be calibrated so that one of the peaks has zero frequency, since only the separation is important.

To interpret the Fabry-Pérot output, the transmitted beam was led into a photo detector coupled to an oscilloscope (Tektronix).

# 3 Setup materials

A lot of equipment was used to carry out the measurements conducted in this project. Power meters from Melles Griot were used to determine pump and laser power, a spectrum analyzer by Agilent helped in studying the absorption/emission/laser spectra and finally, a temperature controller by Tektronix and a diode driver by Profile were used for the cavity setups. For the setups described in sections 4 and 5, external mirrors by Layertec were used as in/outcouplers. When constructing a monolithic laser (section 7, 8 and partly 6), silicone rubber (PDMS) was used as glue. It was a heat curing silicone elastomer (polydimethylsiloxane) made from Sylgard 184 mixed with 10% elastomer curing agent. Moreover, it was degased and then hardended at 85°C. One of the cavity mirrors used was a coated BK7 micro lens made by Edmund optics. Furthermore, a Bragg grating from Optigrate was used as the second mirror, the material for the grating being glass. The used property values for the monolithic components are listed in table 3.1. The values of the lens and grating are stated by the providers apart from the grating $\alpha_T$ which was experimentally found (see section 7). The value stated is actually the sum of $\alpha_T$ and $dn/dT \cdot 1/n$, called $\alpha_{T,eff}$.

| | **Incoupling lens** | **Volume Bragg grating** | **PDMS** |
|---|---|---|---|
| Dimensions | Φ: 3 mm<br>$d_c$: 1.08 mm<br>ROC: 6.2 mm | 3*5*5 mm | - |
| Refractive index $\eta$ | 1.517 | 1.49 | 1.43 [15] |
| Thermal exp. coeff. $\alpha_T$, $[\cdot 10^{-6}/°C]$ | 7.1 | 9.4 | - |
| Thermo-opt. coeff. $d\eta/dT$, $[\cdot 10^{-6}/°C]$ | 2.1 | - | - |

***Table 3.1.*** *Properties of the pieces used in the monolithic setups.*

## 3.1 Absorption

One fundamental concept of a laser is absorption. When pumped, the lasing medium can absorb the pump photons corresponding to an electronic energy transition from the groundstate. As the pump light progresses through the

medium, it will hence be absorbed, according to the Beer-Lambert law [4]

$$I = I_{in} e^{-\sigma_{abs} N z}, \tag{3.1}$$

where $I$ is the transmitted intensity, $I_{in}$ is the incident intensity, $\sigma_{abs}$ is the absorption crossection, $N$ is the absorbant number density and $z$ is the distance traveled through the absorbing media. The factor $\sigma_{abs}N$ is also known as the *absorption coefficient*, or $\alpha$.

### 3.1.1 Doping concentration

The absorbing atoms or ions are *doped* into a host material, usually a crystal or glass material. As discussed in the previous paragraph, the number density $N$, or the doping concentration, is of great importance to the absorption. If assumed that all doped $Nd^{3+}$ ions are in their groundstate when not pumped, and that they all will interact with the pump light, the number density $N$ will thus equal the doping concentration $N_{Nd}$ for both glass and crystal, and the absorption coefficient $\alpha$ will be

$$\alpha = \sigma_{abs} N_{Nd}. \tag{3.2}$$

#### 3.1.1.1 Doping in glass

To find the doping concentration $N_{Nd}$ in the glass, i.e. the number of $Nd^{3+}$ ions per volume, the doping factor $p$ is used. For an inhomogenous material such as glass, $p$ is usually referred to as the mass ratio, $p = m_{Nd}/m_{tot}$, where $m_{Nd}$ is the neodymium mass and $m_{tot}$ is the mass of the doped host. For the glass used, $p = 8\%$. Hence,

$$N_{Nd} = \frac{\rho p}{m_{Nd} m_{kg}}, \tag{3.3}$$

where $\rho$ is the mass density of the host, $m_{Nd}$ is the atomic mass of Nd (actually $Nd^{3+}$, but the removal of three electron masses can be neglected) which is 144.24 u and $m_{kg} = 1.66054 \cdot 10^{-27}$ kg/u is the conversion factor from atomic mass to mass [3].

#### 3.1.1.2 Doping in $GdVO_4$

In the case of a $GdVO_4$ being the host material , $p$ is not the mass ratio of Nd to host mass as in the case of glass. It is simply the ratio of Gd atoms being switched to $Nd^{3+}$ ions, called *atomic doping*. Hence, a doped unit means the removal of the Gd from one unit of $GdVO_4$ and addition of one $Nd^{3+}$ unit. Here $p = 0.5at.\%$. Using $m_{crystal} = 272.2$ u [3], the atomic mass of one unit of $GdVO_4$, equation 3.3 has to be rewritten into

$$N_{Nd} = \frac{\rho p}{m_{crystal} m_{kg}}. \tag{3.4}$$

## 3.2 Gain media

This project is focused on neodymium ions $Nd^{3+}$ as the absorbants, doped into a host material. Fig.3.1 shows the energy levels of $Nd^{3+}$, doped into YAG crystal [1]. The wavelengths differ somewhat with other hosts, but are principally the same.

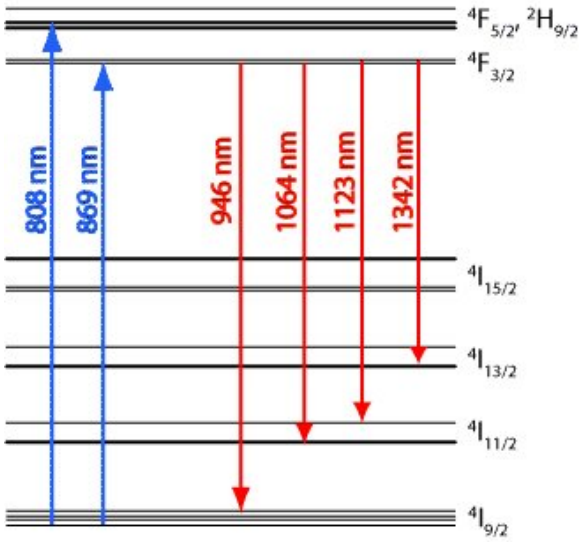


***Figure 3.1.*** *Energy levels of $Nd^{3+}$ with corresponding wavelength transitions in Nd:YAG. Comparable to Nd:glass and Nd:$GdVO_4$ [1].*

### 3.2.1 Host material properties

During this project, two different types of gain media were used. One was neodymium doped into phosphate glass, Nd:glass, and the other one was neodymium doped into the crystal gadolinium vanadate, Nd:$GdVO_4$. They posses somewhat different properties relative to one another due to the different host materials. The $Nd^{3+}$ doping factors used were 8% (mass ratio) for the glass host, and 0.5at.% for the crystal. The main characteristics are found in table 3.2. Some of the values are stated by the providers, whereas others are found in the references stated. The absorption crossections are experimentally attained as shown later in this section.

#### 3.2.1.1 Advantages and disantvantages of the hosts

Most solid state lasers of today use doped crystals as gain medium, i.e. an absorbant doped into a crystalline host. The benefits of these materials are numerous, such as the narrow bandwidth lasers produced as well as high

| **Properties** | **Nd:glass** | **Nd:$GdVO_4$** | |
|---|---|---|---|
| | | $\pi$-pol(c) | $\sigma$-pol(a) |
| Emission crossec. $\sigma_{em}$, [$\cdot 10^{-20}$ cm$^2$] | 4.3 [6] | 125 [10] | 61 [10] |
| Absorption crossec. $\sigma_{abs}$, [$\cdot 10^{-20}$ cm$^2$] | 1.2 | 4.1 | 0.7 |
| Refractive index $\eta$ | 1.503 | 2.2 [10] | 2.0 [10] |
| Thermal exp.coeff. $\alpha_T$, [$\cdot 10^{-6}/°$C] | 7.2 | 7.3 [17] | 1.5 [17] |
| Thermo-opt. coeff. $d\eta/dT$, [$\cdot 10^{-6}/°C$] | -0.4 | 4.7 [17] | |
| Density $\rho$, [g/cc] | 2.60 [6] | 5.47 | |
| Fluorescent lifetime $\tau$, [$\mu$ s] | 330 [6] | 107 [13] | |

***Table 3.2.*** *The most important material properties for the glass and crystal hosts. The two values for Nd:$GdVO_4$ correspond to the $\pi$ and $\sigma$-polarizations respectively. (c) and (a) stand for the crystal c and a-axis. $\sigma_{em}$ is @1064 nm and $\sigma_{abs}$ is @808 nm. The $\tau$ are the lifetimes of the upper laser level $^4F_{3/2}$.*

power pumping possibility. Growing these crystals however, is often time consuming and costly. Furthermore, due to the crystalline structure, it is very difficult to make large pieces and hence difficult to make large lasers. If one uses a glass material as a host instead, it would be possible to greatly reduce the costs as well as the size limitations of the gain medium. Some of the main advantages/disadvantages are found in the table below [1,2].

| | Nd:glass | | Nd:$GdVO_4$ |
|---|---|---|---|
| + | Cheap | +(-) | Narrow bandwidth |
| + | Easy to produce | + | Fairly low thresholds |
| + | Ability for large pieces | + | Good thermal conductor |
| + | More flexible material, e.g. for fibers | + | High power lasers |
| + | Low scattering losses for composite gain media | | |
| - | Poor thermal properties | - | Expensive |
| - | Higher threshold values | - | Hard to grow large pieces |
| -(+) | Broad bandwidth | - | Low versatility |
| | | - | High scattering losses for composite gain media with glass |

The two last advantages listed for the glass host are the ones of most interest

for this project, and the reason why glass and not only crystal was to be used. The benefit of glass instead of crystal is being an easy material to work with. It would for example be possible to write a grating directly into the glass gain medium, which can be useful for wavelength locking purposes when building monolithic lasers. An integrated grating leads to no reflection losses in the interface grating - gain medium, as would be the case if one had to combine them as two separate pieces.

#### Thermal damage threshold

The poor thermal properties of the glass host was also of large importance. This property limits high output powers since the host material is damaged before reaching high pump powers. The medium used here had a damage threshold at just under 240 mW of absorbed c.w. pump power with a pump focus of 40 $\mu$m and a glass temperature of 17°C. Larger focus of course means higher damage threshold since the intensity upon the glass will decrease, but the goal monolithic cavity should have a focus of 40 $\mu$m, so this was the case studied. The damage threshold didn't show much difference when changing the temperature of the crystal.

### 3.2.2 Spectroscopic measurements

In order to determine the pump wavelength needed, spectroscopic measurements of the glass and crystal were carried out. The doped glass and Nd:$GdVO_4$ were illuminated by an ordinary light bulb, i.e. white light, and the transmitted light was studied through a spectrum analyzer. The absorption spectra can be seen in Fig.3.2 and 3.5. Equivalently, to attain the emission spectra the media were shone on by the pump laser at the absorption wavelength, after which the emission was studied by the same analyzer. To get the values of the absorption crossection $\sigma_{abs}$, the absorbed pump was studied. Using the Beer-Lambert law, Eq.3.1, $\alpha$ was found and by knowing $N_{Nd}$, $\sigma_{abs}$ could also be determined by Eq.3.2.

#### 3.2.2.1 Absorption and emission of Nd:glass

The absorption peak of interest in Fig.3.2 is the one at 801 nm. It is thus apparent that the main absorption is somewhat displaced from the 808 nm peak of Nd:YAG. The full width half maximum of the absorption bandwidth, FWHM, was determined to 20.8 nm which is a fairly large value. Consequently, the pump wavelength doesn't have to be exact for efficient excitation. The 801 nm peak and the one around 870 nm corresponding to the transitions $^4I_{9/2} \rightarrow^4 F_{5/2'}$ and $^4I_{9/2} \rightarrow^4 F_{3/2}$ respectively, can be seen in Fig.3.1. The wavelengths differ slightly however due to the difference in host material.

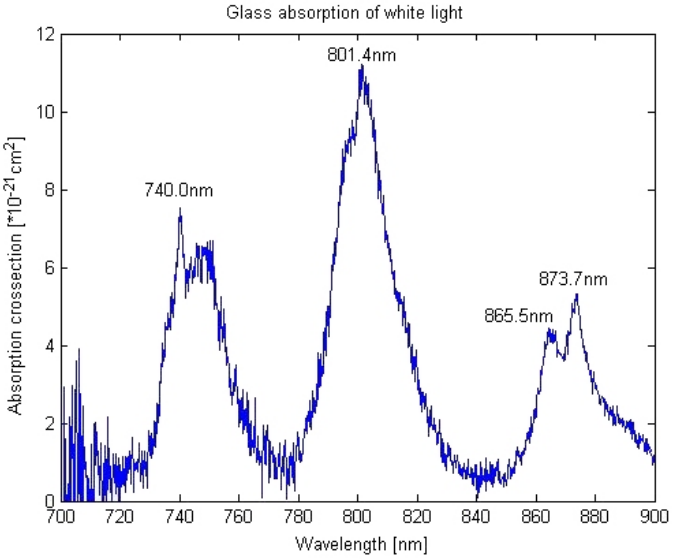


***Figure 3.2.*** *Absorption crossection vs. wavelength showing absorption peaks in a 1 mm thick glass sample.*

The emission of the Nd:glass was also studied, and the result can be seen in Fig.3.3(a). The peak at 1054 nm is the one of interest for this project, and originates from the transition ${}^4F_{3/2} \rightarrow {}^4 I_{11/2}$. A closeup of the 1054 nm peak can be seen in Fig.3.3(b), and shows a FWHM bandwidth of ∼15 nm.

### Theoretical and experimental $\alpha$ of Nd:glass

Taking the logarithm of Eq.3.1 yields

$$\log I = \log I_{in} - \alpha z. \tag{3.5}$$

The above expression describes a linear dependence in the logarithm of the intensity, thus also the power, and the path length $z$ through the gain media. Using this relation, one can find the value of $\alpha$ as the slope of the logarithm of the transmitted power vs. the thickness $d$ of the glass. Hence, the pump power after the glass sample was measured for three different samples (with different thicknesses), to attain the transmitted power. From the gathered data the experimental value of the absorption coefficient $\alpha_{exp}$ was found to be 9.1 $\text{cm}^{-1}$, as seen in Fig.3.4. Knowing $\text{N}_{Nd}$ by Eq. 3.3, as well as table 3.2, $\sigma_{abs}$ is determined by the use of Eq. 3.2. It is $12.2 \cdot 10^{-21}$ $\text{cm}^2$ at a pump wavelength of 801 nm.

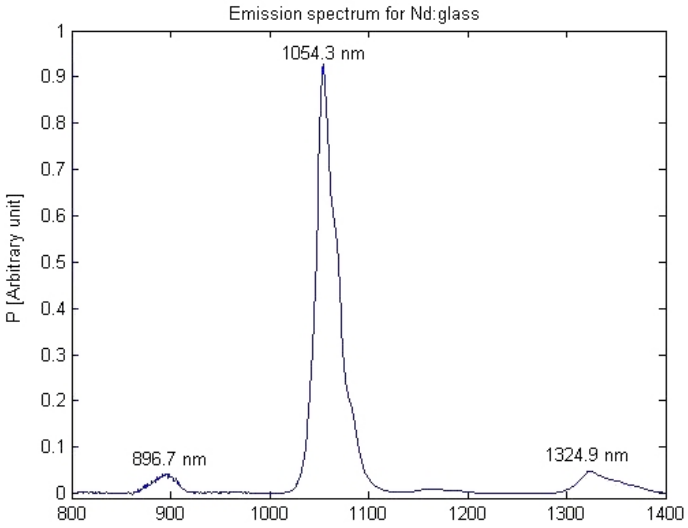


***(a)*** *The whole emission spectrum of the Nd doped glass.*

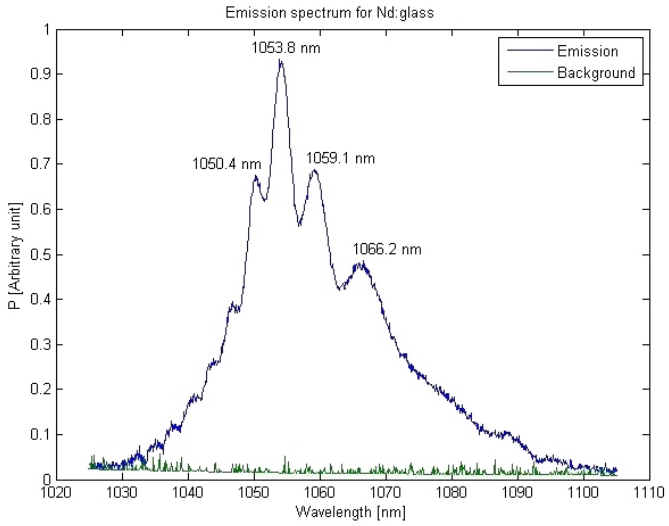


***(b)*** *The emission spectrum around the 1054 nm peak.*

***Figure 3.3.*** *Emission spectra of Nd:glass.*

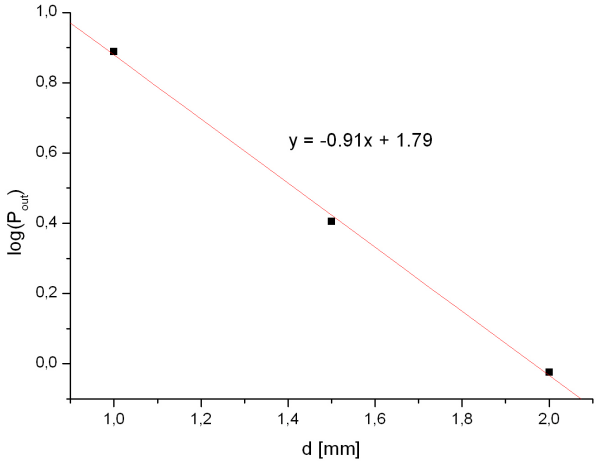


***Figure 3.4.*** *The logarithm of the transmitted pump power vs. the thickness of the glass at a fixed pump power. The slope represents the value of* $\alpha$.

#### 3.2.2.2 Absorption and emission of Nd:$GdVO_4$

The emission and absorption of Nd:$GdVO_4$ are more complex compared to Nd:glass. Due to the crystalline structure of $GdVO_4$, it has three perpendicular axes, namely two a-axes and one c-axis. The absorption is coupled to the polarization of the pump light, so that it peaks when the pump polarization is parallel to the c-axis. This is referred to as $\pi$-polarization, whereas perpendicular pump to c-axis is known as $\sigma$-polarization. The above denomination is valid for the emission as well, with the modification that the emitted light, rather than pump light, is polarized either parallel or perpendicular to the c-axis.

The absorption spectra for both the pump $\pi$-pol and $\sigma$-pol are shown in Fig.3.5. In order to get the results for the two different polarizations, a glan polarizer was used before the crystal. The same was done to get the emission spectra, but with the polarizer after the crystal instead. The FWHM bandwidth of the $\sim$808 nm peak is found to be roughly 15 nm for both cases. Fig.3.6 shows the emission spectrum of Nd:$GdVO_4$ in the $\pi$-pol. The 880 nm peak originates from the ${}^4F_{3/2} \rightarrow {}^4 I_{9/2}$ transition, the 1063 nm peak from ${}^4F_{3/2} \rightarrow {}^4 F_{11/2}$ and the 1341 nm peak comes from the ${}^4F_{3/2} \rightarrow {}^4 I_{13/2}$ transition. The emission peaks don't always match the energy levels in Nd:YAG precisely, due to the different host material compared to the YAG crystal in Fig.3.1. The interesting peak for this project is the one at 1.06 $\mu$m, and is seen in more detail in Fig. 3.7. The FWHM

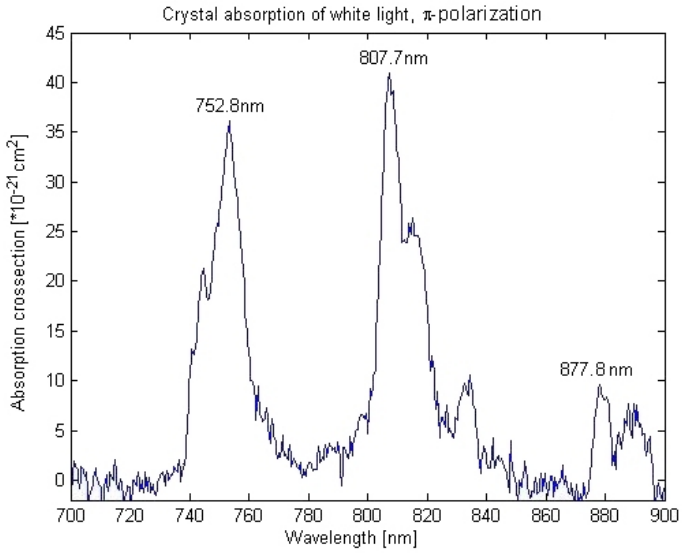


*(a)* $\pi$*-pol.*

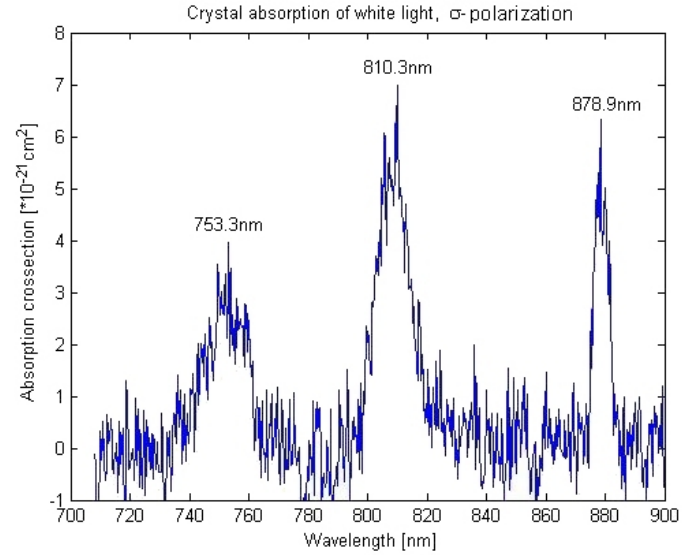


*(b)* $\sigma$*-pol.*

***Figure 3.5.*** *The absorption spectra of* $Nd{:}GdVO_4$ *for the two different pump polarizations.*

bandwidths are around 1.5 nm for both polarizations.

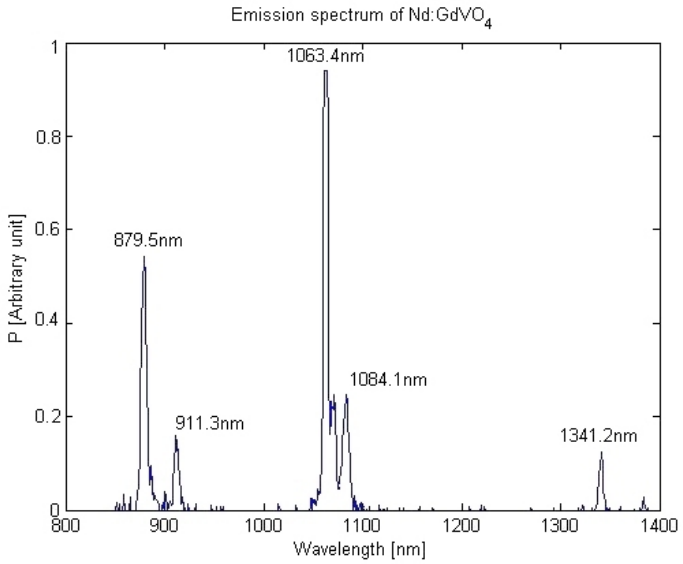


***Figure 3.6.*** *The emission spectrum of Nd:GdVO$_4$ in the $\pi$-pol.*

### Absorption coefficients in Nd:GdVO$_4$

As mentioned in section 3.2.2.2, Nd:GdVO$_4$ has two axes of interest. Hence, there will be two absorption coefficients; one for the $\pi$ and one for the $\sigma$ direction respectively.

Using Eq.3.5, and plotting the transmitted power vs. the length of the gain medium, would require many samples of the crystal with different thicknesses. This was the case for the glass material, but not for the GdVO$_4$. Instead, the Beer-Lambert law was used in another way. The ratio between the transmitted and incident pump power will equal $e^{-\alpha z}$, where z will be the crystal thickness and is thus fixed. The absorption coefficient can hence easily be determined by measuring the two pump powers (this was done for both polarizations of the crystal). The larger absorption corresponds to the $\pi$-pol, and $\alpha_\pi$ was found to be 2.5 cm$^{-1}$. The lower absorption belongs to the $\sigma$-pol, with an $\alpha_\sigma$ of 0.4 cm$^{-1}$.

Using the values in table 3.2 in Eq.3.4 and 3.2, values of $\sigma_{abs}$ are found. For the two polarizations, $\sigma_{abs,\pi}$ and $\sigma_{abs,\sigma}$ are $41 \cdot 10^{-21}$ cm$^2$ and $7 \cdot 10^{-21}$ cm$^2$ respectively at 808 nm.

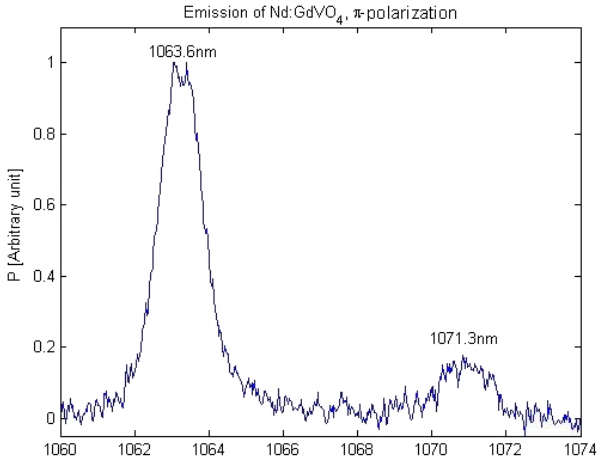


***(a)*** *$\pi$-pol.*

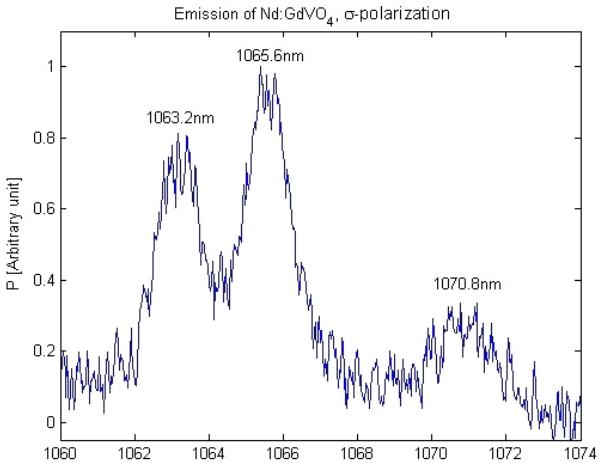


***(b)*** *$\sigma$-pol.*

***Figure 3.7.*** *The emission spectra of Nd:$GdVO_4$ for the two different polarizations, around the 1064 nm peak.*

## 3.3 Diode pump laser

Very often diode lasers are used as pump lasers when constructing solid state laser setups. A diode laser, or laser diode, is a semiconductor laser where the optical gain is generated by a current flowing through a *p-n* junction [1]. The semiconductor material is doped with atoms of one less or one more valence electron than the semiconductor, known as *p-type* and *n-type* materials respectively. In the *p-type* material, *holes* are the charge carriers found in the valence band, whereas electrons are the carriers in the *n-type* material, found in the conduction band. The two regions are then combined, one with excess holes and one with excess electrons. Due to the difference in electron concentration, i.e. *carrier density*, in the $p$ and $n$ regions respectively, there will be a potential difference over the junction [7]. See Fig.3.8 for a graphical explanation. The excess electrons from the $n$ region will flow to the $p$ region at the interface, creating a current over the junction in the opposite direction. Thus, when an electron from the $n$ region *recombines* with a hole in the $p$ region, there will be an energy drop corresponding to the energy difference between the conduction and valence band. The recombination can occur as undesired phonon relaxations, but also, and hopefully as light radiation. This emitted radiation is equivalent to spontaneous emission of the atom, and can thus be used to produce a laser output. As the holes of the $p$ region are filled by the $n$ region electrons, the voltage across the junction decreases. In order to prevent ceasing of the recombination process, an external voltage opposite the junction voltage is applied, forcing the electrons back to the conduction band enabling the process to continue [4].

### 3.3.1 Beam divergence

Looking at Fig.3.8, one can see the depletion layer $d$ as being a very narrow band surrounding the interface between the $p$ region and $n$ region, or *p-n* junction. The recombination occurs in this layer. The magnitude of the depletion layer $d$ is significantly smaller than $h$, the dimension of the semiconductor. Hence, since the emitted light originates from this region, it can be compared to the beam waist of the laser. Using Eq.2.5, where the beam waist $2W_0$ will be the depletion layer d, the total divergence angle $\Theta$ is

$$\Theta = \frac{4\lambda}{\pi d}. \tag{3.6}$$

Here $M^2$ was set to 1. If assumed that the depletion layer will have a magnitude in the order of $\mu$m, this will result in a total divergence angle of over 80°. The laser output from the diode will thus be heavily diverged in the plane across the junction, and a lot less in the perpendicular direction parallel along the junction. Hence, the laser beam will be very elliptical, as

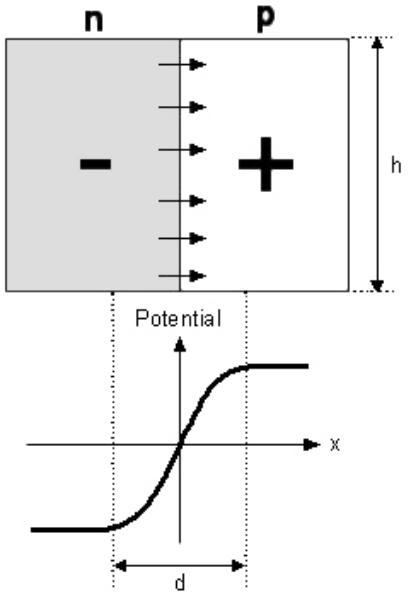


***Figure 3.8.*** *The p-n junction in a semiconductor. Electrons will flow from the p to the n region due to the potential difference. The distance d is known as the depletion layer.*

seen in Fig.3.9. The faster diverging axis is referred to as the *fast axis*, and the other one as the *slow axis*.

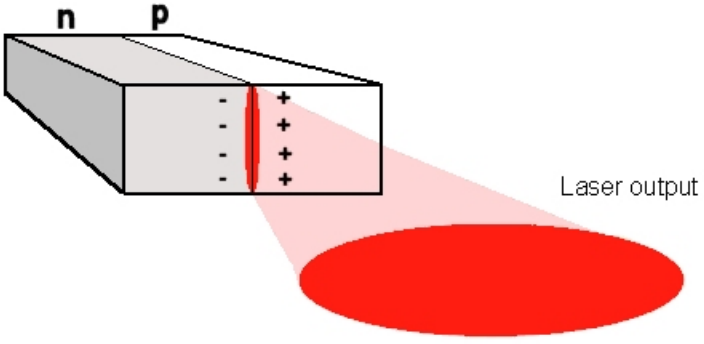


***Figure 3.9.*** *Qualitative description of the divergence of the diode laser.*

### 3.3.2 Pump setup

The laser diode used for this thesis was a LDX-3415-808 from *LDX Optronics Inc.* Its operating wavelength is somewhat tuneable by adjusting the temperature of the diode. For driving currents ranging from 0 to 3.7 A, it was operated at 801 nm up to 808 nm. Since the wavelength changed with drive current (temperature), the absorbed power instead of the pump power is most often used from now on (not to get less absorption due to different pump wavelength for different pump powers). The pump beam was collimated and focused through a series of lenses, shown in Fig.3.10. The third

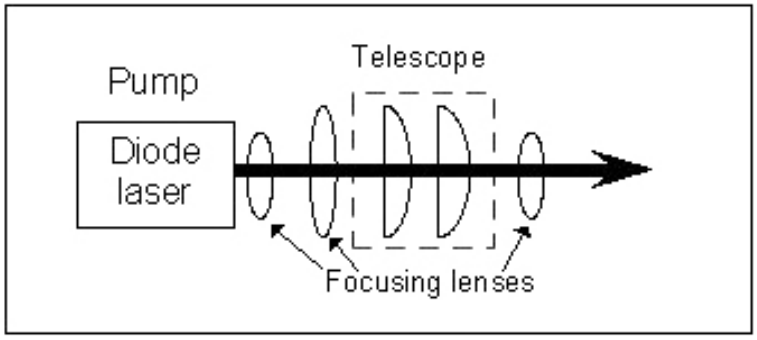


***Figure 3.10.*** *Schematic view of the pump setup.*

and fourth lens are setup like a telescope, and both are cylindrical in order to make the fast axis and slow axis focii described in the previous paragraph coincide and be of equal size. After that, the beam is led into a powerful positive lens with the purpose of strongly focusing the beam and making it symmetrical. The pump beam waist is located roughly 10 mm after the last focusing lens, and has a $1/e^2$-radius of about 40 $\mu$m in the fast axis and 35 $\mu$m in the slow. Using the knife edge technique, measurements of the focii were made. The diode has a very divergent focus, seen in Fig.3.11 which is a plot of the beam waist $\omega$ as a function of location $z$. This suggests that the approximation of constant pump size throughout the gain medium is only valid for thin pieces. The distance separation between the fast and slow focii originate from the measuring equipment, and not from the pump. In reality, they coincide. Using a glan polarizer, the beam was found to be polarized parallel to the slow axis, defined as $\pi$-polarized when working with the crystal gain medium.

#### 3.3.2.1 Diode power output

The diode is driven by a current unit. It can take drive currents as high as 3.7 A. The range used for the experiments conducted here was 0-3.7 A. In

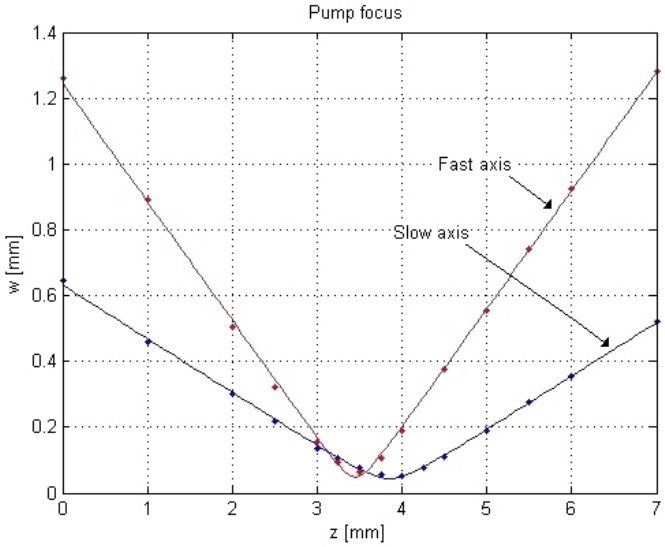


***Figure 3.11.*** *Pump beam waist $\omega$ vs. distance $z$ for the fast and slow axis. The pump focii (w) are 40 $\mu m$ and 35 $\mu m$ respectively.*

order to be able to calculate absorbed powers of the gain media and such, the relation between driving current and pump power had to be measured. It was done by changing the drive current and focusing the pump beam into a power meter, using a positive lens. The results can be seen in Fig.3.12. The driving threshold where the diode starts lasing is found to be roughly 400 mA, and the pump power $P_{pump}$ follows the relation

$$P_{pump} = 0.994W/A \cdot I_{drive} - 377mW, \tag{3.7}$$

where $I_{drive}$ is the driving current. Note that this is relation is valid after the light has passed the series of lenses discussed in the previous paragraph. Accordingly, Eq.3.7 doesn't describe the direct output of the diode, but the output of the entire pump setup depicted in Fig.3.10. Eq.3.7 will be used throughout the experiments, converting diode drive current to diode pump power.

## 3.4 Volume Bragg gratings

There is often a need for narrow width lasers, with the further advantage of being stable and compact. One way to achieve these demands is to use a volume Bragg grating as outcoupler (or incoupler) in the cavity setup. Based on periodicity, a Bragg grating has a periodic perturbation of the refractive index (see Fig.3.13), causing very large reflectivity for the wavelength

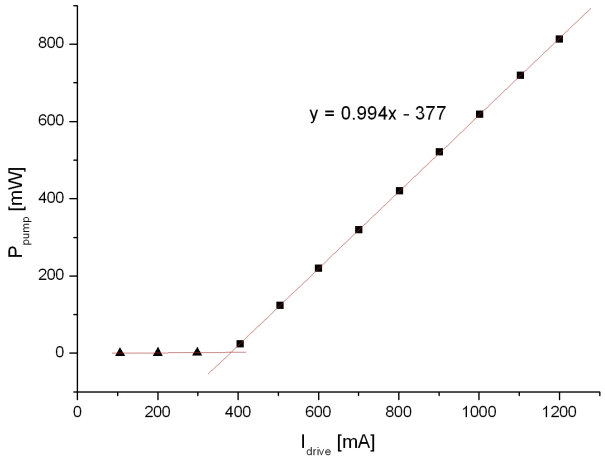


***Figure 3.12.*** *Pump power vs. driving current. The driving threshold is at roughly 400 mA.*

fulfilling the *Bragg condition* [12]:

$$\lambda_B = 2n_0 \Lambda cos\theta, \tag{3.8}$$

where $\lambda_B$ is the Bragg wavelength, $n_0$ the central index of refraction of the volume medium, $\Lambda$ is the grating period and $\theta$ is the incident angle upon the grating, depicted in Fig.3.14. The volume material here was a glass with refractive index 1.49. Apart from the bandwidth narrowing, the volume grating has further advantages, such as high optical damage threshold and no noticeable degradation over time despite heavy use. Furthermore, by adjusting the grating period virtually any Bragg wavelength can be reached [12].

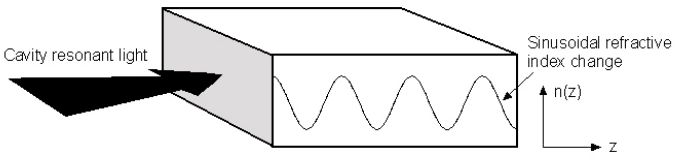


***Figure 3.13.*** *Qualitative description of the sinusoidal change in refractive index $n(z)$ at a distance $z$ into the Bragg grating.*

### 3.4.1 Reflective properties

The results of the credited paper by Kogelnik [16] has been widely used to describe the reflective properties of Bragg gratings. The results are as old as 40 years, but still give a valid description. They are achieved in the plane-wave approximation and under the assumption that a grating of length $L$ has a sinusoidal refractive index variation with amplitude $n_1$ and period $\Lambda$ around a constant index $n_0$, $n(z) = n_0 + n_1 sin(n\pi z/\Lambda)$ [11]. Furthermore, an internal angle of $\theta$ between the incident light wave vector $k$ and the grating vector $K = 2\pi/\Lambda$ is assumed, depicted in Fig.3.14. Note that $\theta$ will be the angle between $k$ and $K$ inside the grating medium, so under circumstances other than normal incidence Snell's law has to be applied to the incident light first. Eq.3.8 tells us that a sinusoidal variation will give a reflection

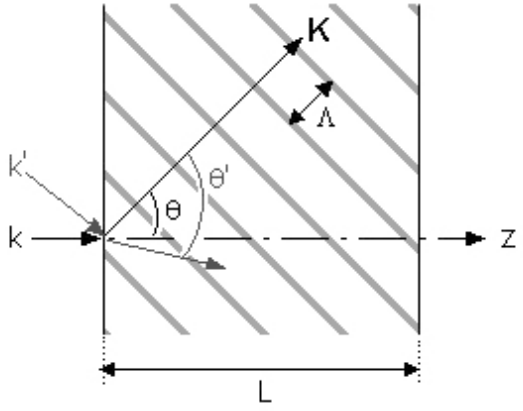


***Figure 3.14.*** *The most important quantities concerning Bragg gratings.*

at the Bragg wavelength $\lambda_B = 2n_0\Lambda cos\theta$ (i.e. the wavelength at maximum grating reflectivity). Hence, under the above assumptions, the electric field amplitude $r = \sqrt{R}e^{i\varphi}$ for a wave vector slightly off the the Bragg peak at $k_B$, $k = k_B + \delta k$ is given by [11]

$$R(k,\theta) = \begin{cases} \frac{\kappa^2 sinh^2(\alpha L/cos\theta)}{\kappa^2 cosh^2(\alpha L/cos\theta) - (\delta k cos^2\theta)^2} & |\delta k| < \kappa \\ \frac{\kappa^2 sin^2(|\alpha| L/cos\theta)}{-\kappa^2 cosh^2(|\alpha| L/cos\theta) - (\delta k cos^2\theta)^2} & |\delta k| > \kappa, \end{cases} \tag{3.9}$$

$$\varphi(k,\theta) = \begin{cases} -arctan(\frac{\delta k cos^2\theta}{\alpha} tanh(\alpha L/cos\theta)) & |\delta k| < \kappa \\ -arctan(\frac{\delta k cos^2\theta}{|\alpha|} tan(|\alpha| L/cos\theta)) + m\pi & |\delta k| > \kappa. \end{cases} \tag{3.10}$$

where $\alpha = (\kappa^2 - (\delta k cos^2\theta)^2)^{1/2}$, with the grating strength being $\kappa = n_1 k/(2n_0) = n_1\pi/\lambda$ and $m$ is an integer determining order. Also, the incident light wave vector is $k = 2\pi n_0/\lambda$ and the Bragg wave vector is

$k_B = 2\pi n_0/\lambda_B$. The deviation from the peak wavelength, $\delta k$ is known as the *detuning*, leading to zero detuning simply meaning $\delta k = 0$. Here zero detuning corresponds to zero phase $\varphi$.

At zero detuning for normal incidence, i.e. $\delta k = \theta = 0$, we find the peak reflectivity at a value of $R_{max} = tanh^2 \kappa L$. Also, the spectral distance between the two minima closest to the peak reflectivity, i.e. the spectral bandwidth $\Delta\lambda$ at normal incidence, is [11]

$$\Delta\lambda = \lambda_B({n_1}^2/{n_0}^2 + 4\Lambda^2/L^2)^{1/2}. \tag{3.11}$$

Note that this bandwidth is defined as the bottom width (to the first zeros) and not as the normal full width half maximum. Measuring the reflectance and transmittance of the grating used in this project, one finds the result shown in Fig.3.15. From the data, it is found that $R_{max}$ is $\sim 99.5\%$. The FWHM spectral bandwidth is around 0.2 nm for the reflectivity, with a peak at around 1066.1 nm. $\Lambda$ can be found by the measured Bragg wavelength and Eq.3.8, and by Eq.3.11 the refrative index amplitude modulation $n_1$ is determined to $2.2 \cdot 10^{-4}$ [11].

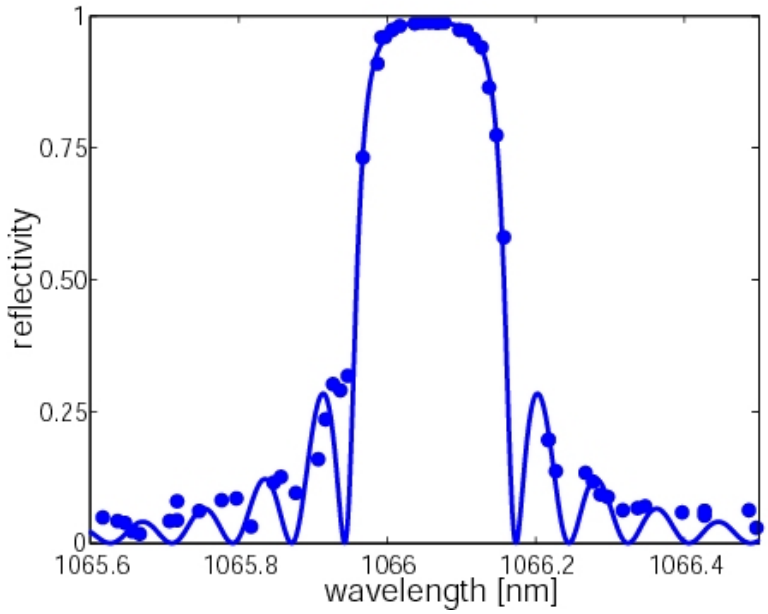


***Figure 3.15.*** *Reflectance R at different wavelengths for the Bragg grating.*

### 3.4.2 Effective grating length

When studying Eq.3.10, it is noted that the phase varies very modestly, i.e. linear, around the peak [11]. At normal incidence, the phase is

$$\begin{aligned} \varphi &= -arctan(\frac{\delta k}{\alpha} tan(\alpha L)) \\ &= -arctan(\frac{\delta k/\kappa}{\sqrt{1-(\delta k/\kappa)^2}} tan(\sqrt{1-(\delta k/\kappa)^2}\kappa L). \end{aligned} \tag{3.12}$$

Based on this, a Taylor expansion at normal incidence around zero detuning is made, for the detuning $\delta k/\kappa$, yielding

$$\varphi(\delta k/\kappa) = -\sqrt{R_{max}}\delta k/\kappa + O((\delta k/\kappa)^3). \tag{3.13}$$

This is thus an approximation of the phase $\varphi$ around the peak. If one instead considers the phase change of the wave with $k = k_B + \delta k$ traveling the distance $\Delta L$ in a medium, then the phase change will be $\varphi = (k_B + \delta k)\Delta L$. Only the detuning $\delta k$ will contribute to the phase change, since the $k_B$ part only gives a constant phase which is unimportant. Thus, the total roundtrip distance traveled within the grating medium is equivalent to $\Delta L$, which can also be thought of as two times the effective grating length $L_{eff}$ as shown in Fig.3.16. Accordingly, when discarding the constant phase $k_B\Delta L$,

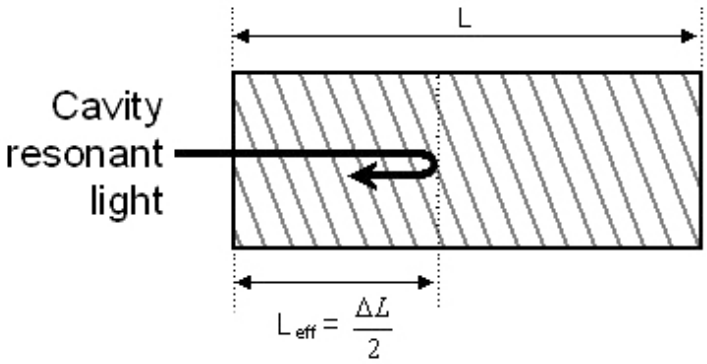


***Figure 3.16.*** *Depiction of the effective grating length $L_{eff}$ compared to the actual length L.*

$2L_{eff} = \Delta L = \pm\varphi/\delta k$. The $\pm$ comes from the fact that the phase changes sign when reflected. Comparing to the phase in Eq.3.13 one finds the relation

$$L_{eff} = \frac{1}{2}\sqrt{R_{max}}/\kappa. \tag{3.14}$$

When using Eq.3.14 with the peak reflectivity of 0.995 shown in Fig.3.15, together with $\kappa = n_1\pi/\lambda$ for $n_1 = 2.2 \cdot 10^{-4}$, the effective grating length $L_{eff}$ is found to be $\sim$0.77 mm.

## 3.5 Cavity reflection losses

Most materials used as gain media in a laser are anti-reflection coated at the laser wavelength in order to minimize cavity losses. If uncoated however, the materials are not fully transmitting the incident light on the in/outcoupling surfaces, plus there will be internal reflections on the material interfaces within the cavity. When the angle of incidence approaches zero, i.e normal incidence, the reflectance $R$ at the interface of two media can be described by

$$R = (\frac{n_2 - n_1}{n_2 + n_1})^2, \tag{3.15}$$

which is a simplification of the Fresnel equation [5]. Here $n_1$ is the refractive index of the first medium and $n_2$ is that of the second. Uncoated surfaces will give rise to reflections according to Eq.3.15 at normal incidence. These reflections are thus lost from the laser intensity within the cavity. To get an idea of the sizes of these losses, 3.15 can be applied to the setup used. The simplest form of cavity with the gain medium surrounded by air and two external mirrors, as well as the compact monolithic laser can be seen in Fig.3.17. The total reflectance will be the sum of all $R_i$ within the cavity. To achieve a good laser output with a large slope efficiency, the outcoupling

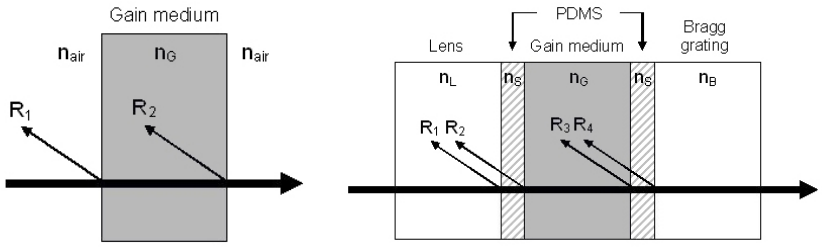


***(a)*** *Reflectance when the gain medium is surrounded by air.*

***(b)*** *Reflectance within the monolithic cavity. The incoupling and outcoupling surfaces are AR coated and are hence neglected.*

***Figure 3.17.*** *Reflection losses of two different types of cavities used in this project. The $n_i$ are the refractive indices of the corresponding material.*

should at least equal the losses (which are mainly reflection losses for the setups in question).

The total cavity loss $\delta$ will be the sum of the outcoupling and the reflection loss. There might also be some other losses, such as scattering

losses within the cavity medium, but these are normally very small when working with a proper laser gain medium.

# 4 Comparing Nd:glass and Nd:$YVO_4$

During the experiments carried out, it became evident that the pumping threshold was of great importance, not least in the case of the Nd:glass media which proved very weak to thermal load. In order to find the threshold value for Nd:glass, to see if it was possible to reach it before damaging the glass, a special experiment was carried out for this sole purpose. To get an estimate of the threshold, some calculations had to be done.

Looking at the rate equations (omitted in this thesis) for the population of the different levels in a four level system, such as $Nd^{3+}$, some derivations can be made. At the laser threshold, the system is in steady state. Using this, one finds an expression for the absorbed pump power at threshold, $P_{th}$ [9]

$$P_{th} = \frac{\pi h \nu_P \delta(\omega_P{}^2 + \omega_L{}^2)}{4\sigma_{em}\tau}. \tag{4.1}$$

The quantities to the right are the Planck constant $h = 6.626 \cdot 10^{-34}$ Js [3], pump frequency $\nu_P$, and the total cavity loss $\delta$. If the reflection loss is denoted $L$ and the transmission loss is $T$, then the loss is the logarithmic loss $\delta = L - ln(1 - T) \approx L + T$ for small T. Further quantities are pump and laser mode size within the cavity, $\omega_P$ and $\omega_L$, emission crossection $\sigma_{em}$, and finally fluorescence lifetime of the upper laser level $\tau$.

By the use of Eq.4.1, an estimate of the threshold value could be determined and compared to the experimentally attained one. The cavity seen in Fig.4.1 was setup, using two different gain media in order to check the validity of equation 4.1. The threshold values for both Nd:glass and Nd:$YVO_4$ as gain media were then looked for.

## 4.1 Experimental setup

The basic setup used for the experiment can be seen in Fig.4.1. The gain medium in the cavity was switched between the Nd:glass sample and the Nd:$YVO_4$. The $\lambda/2$ plate and crystal components were used to change the power output of the pump, instead of directly changing the power supply to the Ti:Saph pump laser, this in order to increase stability. By rotating the $\lambda/2$ plate the polarization of the passing light changes. The glan polarizer is designed to only let a certain polarization through, which hence makes the two work as a power control without absorbing the heat of the pump beam and risk damaging. Another source of instability can be feedback from the cavity back into the pump laser. The Faraday isolator prevents this by only letting a part of the light with a specific polarization through, which will then be stopped from traveling back in the other direction. The pump light is then directed by two mirrors in order to be able to change the height and angle of the beam going into the cavity. The light then reaches the cavity. Both the outcoupling and incoupling mirrors (Layertec) were HR at 1064

nm. The reason for using a HR mirror as an outcoupler, instead of e.g. one with 95% reflectance or such, was to decrease the threshold as much as possible to be able to reach it before damaging the glass medium (∼400 mW pump power). Since the output was not interesting in this setup, it was a mere test, the slope efficiency was not relevant and didn't prevent the use of such low outcoupling. The gain medium was switched throughout the experiment; both Nd:glass and Nd:$YVO_4$ was used.

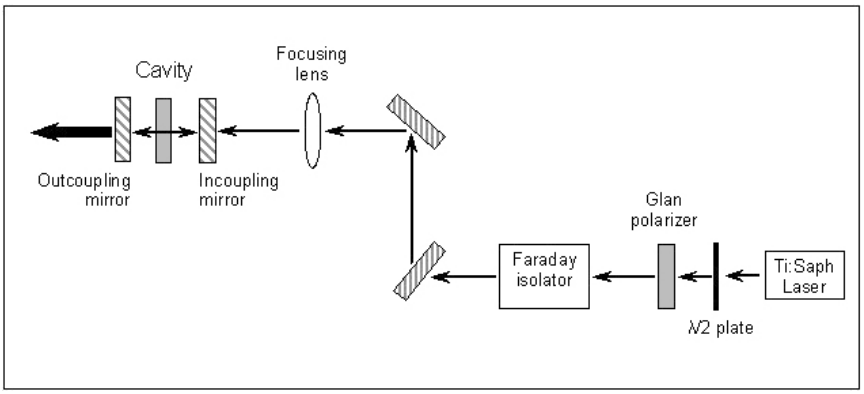


***Figure 4.1.*** *Schematic view of the setup.*

## 4.2 Threshold of Nd:$YVO_4$

For the setup used it was assumed that the pump size was constant throughout the crystal. It was adjusted as to fit the first transversal mode size of the cavity, leading to equal pump size $\omega_P$ and mode size $\omega_L$. WinLase gave a mode size of 164 $\mu$m, the pump beam waist at which the crystal was placed. The output was chosen to 0.05% (HR@1064 nm) and other cavity losses were assumed to be only 1% since the crystal surfaces were antireflection coated, yielding a $\delta$ of 0.0105. Other values used were $\sigma_{em,\pi} = 11 \cdot 10^{-19}$ cm$^2$ [1] and $\tau = 107$ $\mu$s [18]. By equation 4.1 an approximate threshold value is found to be slightly under 10 mW. By plotting (Fig.4.2) the gathered experimental data, one finds the threshold value to be around 25 mW. The two values agree in order of magnitude, and one can assume Eq.4.1 to give a valid answer.

## 4.3 Threshold of Nd:glass

To find the glass medium threshold, the exact same setup as for the Nd:$YVO_4$ was used, only switching the gain medium. Since the end surfaces are uncoated, this yields a reflection loss of 16% for a roundtrip according to Eq.3.15. The theoretical value from Eq.4.1, using the values in table

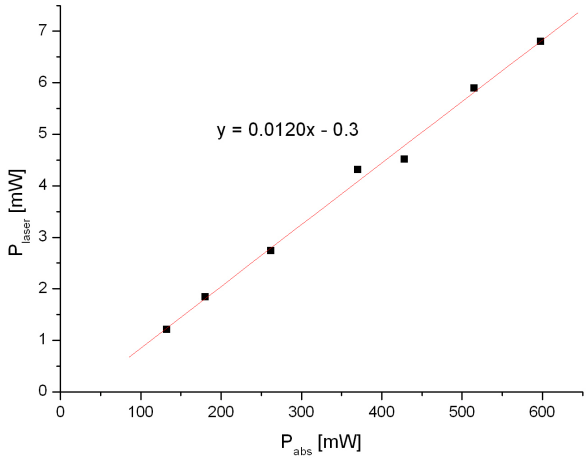


***Figure 4.2.*** *The laser power vs. the pump power. The pumping threshold is roughly 25 mW.*

3.2, reaches almost 1300 mW, which is well above the breaking limit of the glass. In order to minimize these losses in the cavity, the glass was put in it's Brewster angle at around 56° to the cavity resonant light. The $\delta$ will thus be 0.0105 as for the $YVO_4$, if assumed no reflection losses. The new threshold value was found to be 80 mW which is more reasonable. Despite the fairly low pumping threshold, lasing did not occur for the glass cavity for pump powers up to 400mW (or roughly $300mW$ absorbed power, a bit over the damage threshold for a 40 $\mu$m pump focus).

## 4.4 Conclusions

The model of the glass gain medium setup was working in theory, however not in reality. Apparently the material values of the Nd:glass are incorrect. Since the glass setup was unable to lase before reaching it's damage threshold, it was decided not to go any further with the glass material. Not being able to build a working setup for the simplest case with two external mirrors and a larger pump focus allowing some stretching of the damage threshold, was not promising when aiming at a monolithic cavity. Stricter alignment and a smaller pump focus would hardly yield a working setup, hence the part of the project involving the glass medium was terminated.

# 5 Nd-laser with an external mirror

As a first step towards constructing a monolithic, single longitudinal mode laser, a simpler setup was built. Nevertheless, the incoupler was attached to the gain medium, using silicone rubber (PDMS) as glue. Being a mere trial cavity, the output beam quality and power was not of great importance. The main goal was simply to achieve lasing.

## 5.1 Cavity setup and measurements

The basic setup is seen in Fig.5.1. The incoupler used was a HR@1064 nm and HT@808 nm coated BK7 lens ($\eta = 1.517$) with a ROC of 6.2 mm and a center width of 1.08 mm. Despite being a lens, it was used as a mirror due to it's coating. The $0.5at.\%$ Nd:$GdVO_4$ crystal had a 3 by 3 mm clear aperture and a thickness of 2 mm long with other values discussed in section 3, resulting in 40% absorption. It was attached to the incoupler by a very thin layer of PDMS. The outcoupler was a R=95% at 1064 nm, plano-concave mirror with ROC=50 mm from Layertec. To align the cavity, a HeNe laser was used. To keep the transmitted pump from interfering with the measurements, a filter only letting higher IR light through was placed after the outcoupler, blocking only the pump light. In order to measure the power output of the laser, a focusing lens was placed in the output beam, focusing the laser into a power meter. To attain spectra of the laser, the beam was instead focused into a fiber detector coupled to a spectrum analyzer. A glan polarizer was used to determine the output polarization.

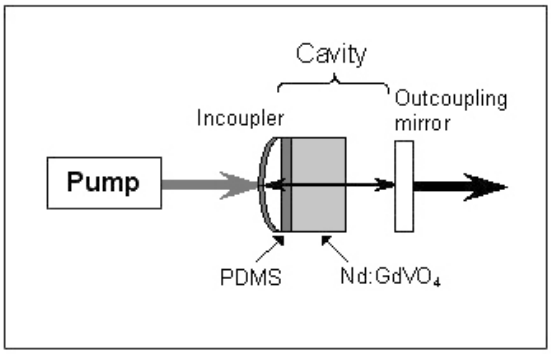


***Figure 5.1.*** *View of the setup. The incoupler is a HR@1064 nm coated lens, glued to the gain medium by a very thin layer of PDMS.*

### 5.1.1 WinLase cavity simulation

In order to construct the most stable and efficient cavity possible, as well as a single transversal mode laser cavity, a model was made as a starting point. Appropriate distances and the gaussian mode size were found, which are necessary facts for the construction. With the help of WinLase [19], cavity simulations could be made and used when building the actual setup. The model can be seen in Fig.5.2 and shows that the mode size is around 40 $\mu$m which agrees with the pump. The mode size poses a restriction on the pump size, since it should not exceed that of the gaussian mode. If it does, you may get multi-transversal modes, which is undesired in this project. Furthermore, it was found that the most stable cavity occurs when the outcoupler is as close as possible to the Nd:$GdVO_4$.

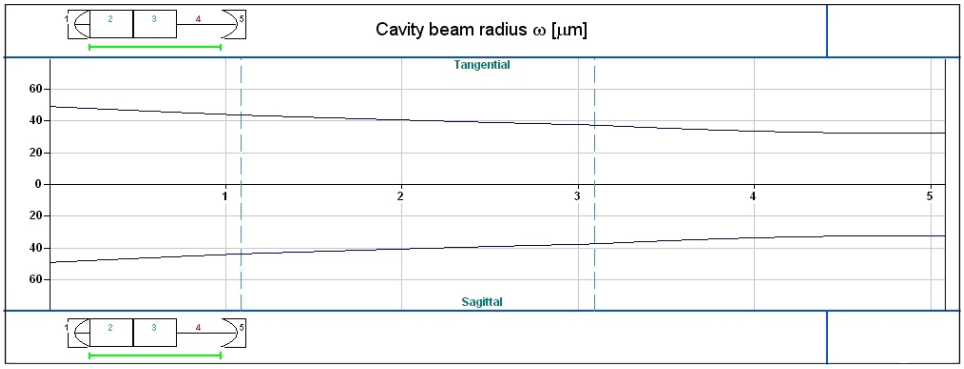


***Figure 5.2.*** *WinLase model of the cavity. The beam radius $\omega$ within the medium is around 40 $\mu$m.*

## 5.2 Results

After some alignment, lasig did occur for the setup. The output peaked at 1063.3 nm, was $\pi$-polarized and operated in multi longitudinal mode as seen in Fig.5.3. Apparently three longitudinal modes oscillate within the cavity, with a mode separation $\Delta\lambda$ of about 0.1 nm. According to Eq.2.15, this corresponds to an optical cavity length of around 5.65 mm, consistent with the real one at $1.08 \cdot 1.517 + 2 \cdot 2 = 5.64$ mm when neglecting the thickness of the PDMS rubber and the tiny distance between the gain medium and the outcoupler. The laser beam was diverging due to the fact that the pump focus was very small ($\sim$40 $\mu$m). This leads to large diffraction effects and thus a diverging beam.

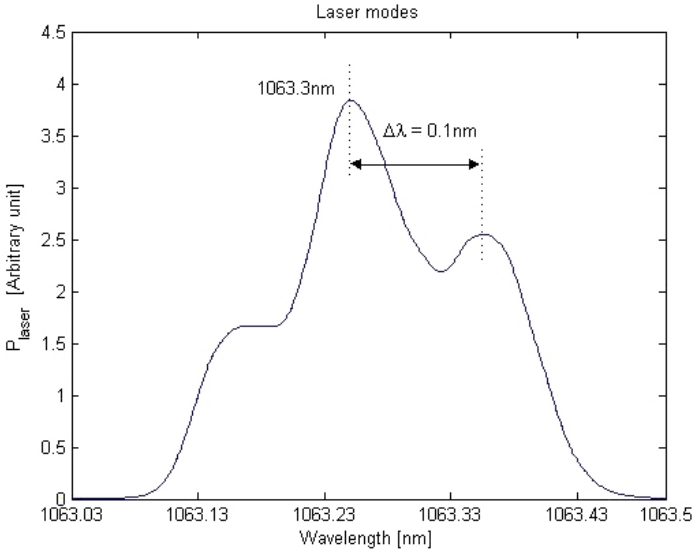


***Figure 5.3.*** *Spectrum of the laser output. Three oscillating modes with a separation $\Delta\lambda$ of about 0.1 nm.*

### 5.2.1 Threshold value of the setup

Measuring the output power of the laser yielded a threshold value of the absorbed pump needed to achieve lasing. A plot of the data collected can be seen in Fig.5.4. For lower pump powers, the threshold value was evaluated to 69 mW. This was the value used, since the laser showed increased instability for higher pump powers, as is also seen in the plot. The slope efficiency $\eta_{eff}$ for the lower powers reached a mere value of 0.032, and 0.092 at higher pump powers. There is obviously an intersection between the two regions, happening just over 700 mW of absorbed pump power in this case. This sudden increase in slope efficiency and power is probably due to higher transversal modes. At a certain limit higher order modes (which have a higher threshold) also start lasing leading to more output power but also a higher $M^2$ value. The intersection is most likely explained by this phenomenon.

Due to the large reflection losses within the cavity, 28% according to Eq.3.15, a larger outcoupling than 5% should have been used. To get a more efficient laser, the outcoupling should have been at least equal to the losses, unattained in this setup.

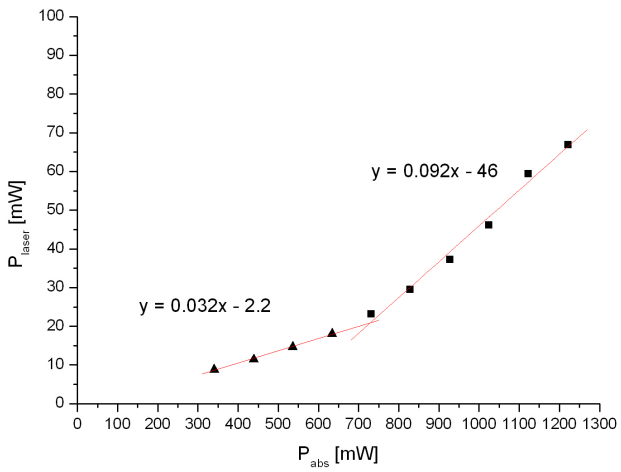


***Figure 5.4.*** *Laser output power vs. absorbed pump power. The threshold value was evaluated to* $69mW$.

# 6 Nd-laser with an external outcoupling, volume Bragg grating

The second step towards the monolithic, narrow band laser was changing the outcoupling mirror in the previous section to a volume Bragg grating. The purpose of operating in single longitudinal mode is a narrower bandwidth as well as a frequency stable laser. As before, the beam quality and power output were of less interest than building a working setup.

## 6.1 Cavity setup and measurements

The setup was basically the same as in section 5, the only difference being the exchange of the outcoupling mirror to a volume Bragg grating, as shown in Fig.6.1. As found in section 3.4, the grating had a peak reflectivity of 99.5% at around 1066.1 nm and an effective grating length $L_{eff}$ of 0.77 mm. Furthermore, the FWHM of the reflection was 0.2 nm and the device was AR coated at 1066 nm. New for this setup was also the use of an extra alignment laser at a wavelength of 1066 nm to properly align the grating, as well as a HeNe one for the incoupler. Since the grating didn't reflect the HeNe laser (633 nm), it couldn't be used for alignment. Having such a narrow reflection band, a laser at it's center wavelength of 1066 nm had to be used to align the grating. To do the measurements of the laser ouput, the pump was blocked using a filter and the laser output beam was focused into a power meter as well as a spectrum analyzer to obtain the power output and laser spectrum respectively. A glan polarizer was used to determine the output polarization.

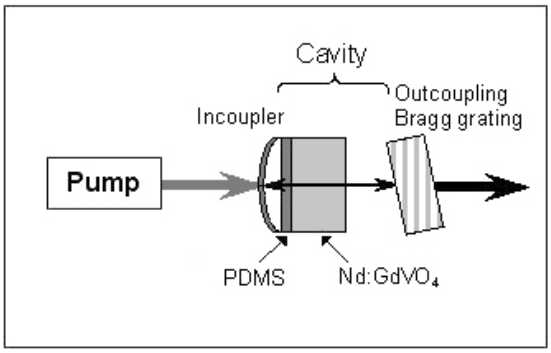


***Figure 6.1.*** *View of the setup. The incoupler is a HR@1064 nm coated lens, glued to the gain medium by a very thin layer of PDMS.*

### 6.1.1 WinLase cavity simulation

Because of the strong focusing properties of the incoupling lens (ROC=6.2 mm), cavity modelling using WinLase showed that the ROC of the outcoupler was of virtually no importance. Thus, the model found in section 5 also holds here, and can be seen in Fig.5.2. We recall that the stability criteria demanded the outcoupler being as close as possible to the crystal gain medium.

## 6.2 Results

As for the previous setup with the external outcoupling mirror, lasing was achieved. This time however, there was not only one laser output beam, but four visible ones. Each material interface contributes with two reflection outputs (in opposite directions); incoupling lens - PDMS (0.09%), PDMS - Nd:$GdVO_4$ (3%) and finally Nd:$GdVO_4$ - air (11%). The three reflections going backwards are reflected by the incoupler to also travel forwards, leading two six reflection outputs apart from the output from the entire cavity rountrip. However, the roundtrip output is only 0.5% compared to the interface reflections, calculated with Eq.3.15. The 0.5% and 0.09% outputs can thus be neglected, and the four outputs are the backwards and forwards reflections from PDMS - Nd:$GdVO_4$ (3%) and Nd:$GdVO_4$ - air (11%), seen in Fig.6.2. Since the PDMS layer was so thin, the reflections from either side of it should almost coincide which was also the case. Two output beams were slightly overlapping. It was possible to attain a laser output at around 1063 nm, but these results were discarded since they meant no coupling to the Bragg grating due to it's narrow reflection band centered at 1066 nm. They were simply oscillations between the incoupler and the gain medium as well as the PDMS.

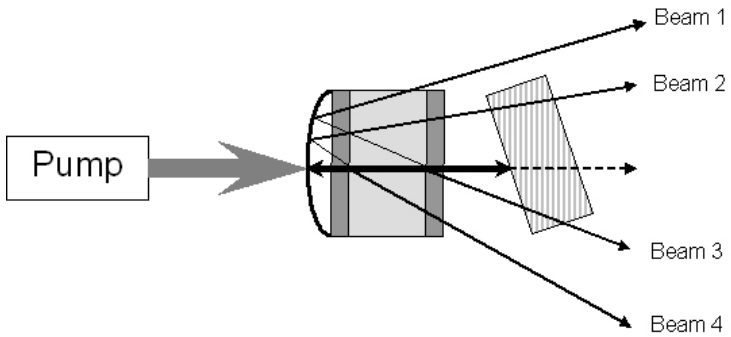


***Figure 6.2.*** *The four output beams originating from interface reflections within the cavity.*

### 6.2.1 Laser spectrum

The laser outputs were found to be $\sigma$-polarized, and a spectrum of one of the beams is seen in Fig.6.3. The main peak of emission is thus at 1066.1 nm. It is also seen that two modes seem to be present, separated by 0.1 nm. Equivalent to the previous section, this corresponds to an optical cavity length of 5.65 mm, compared to the real optical cavity length of $1.08 \cdot 1.517 + 2 \cdot 2 + 0.77 = 6.41$ mm. The reason for the inaccuracy is probably the analyzers resolution. It was just below 0.1 nm which may thus limit the visibility of the actual mode separation.

The output beams were divergent in this setup as well since the pump focus was still as small resulting in diffraction of the beams. Furthermore, the beam quality was fairly low, and higher transverse modes were showing. Being hard to distinguish, the modes were probably $TEM_{01}$, $TEM_{10}$ and/or $TEM_{11}$.

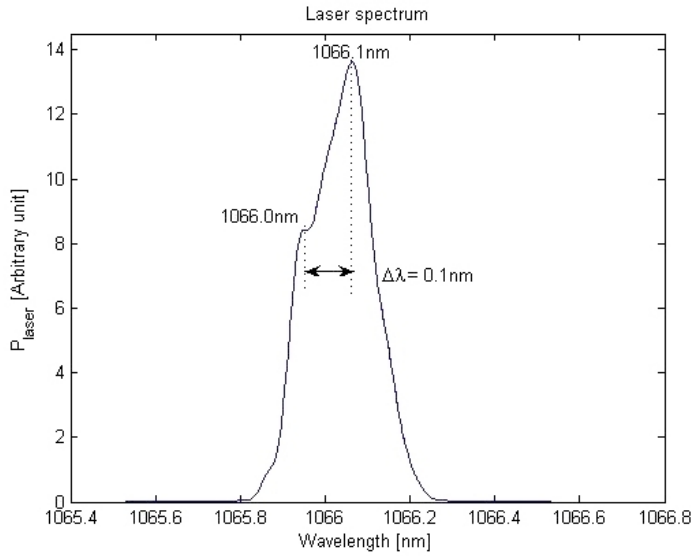


***Figure 6.3.*** *Spectrum of the laser output. The peak is at 1066.1 nm, and the mode separation $\Delta\lambda$ is 0.1 nm.*

### 6.2.2 Threshold value of the setup

A plot of the measurements of the strongest laser output power vs. the absorbed pump power for one of the four beams is seen in Fig.6.4. The threshold value was found to be 820 mW, which is a relatively high value. The slope efficiency on the contrary is unusually low, at a value of 0.089. The outcoupling of 5% was thus not optimal. Furthermore, since the threshold reached such a high value, the typical turning point when the slope efficiency

starts to increase (higher transverse modes start lasing) was never reached.

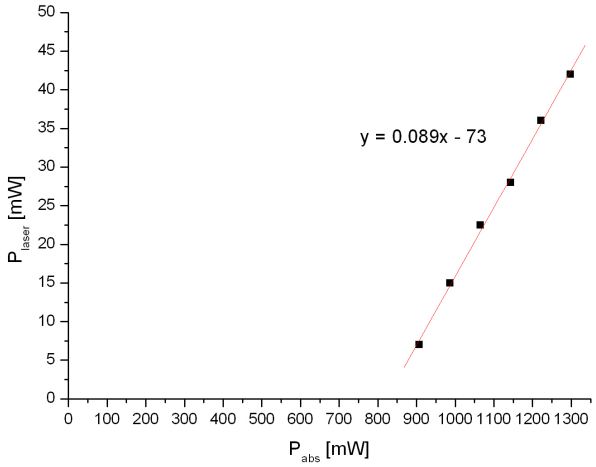


***Figure 6.4.*** *Laser output power vs. absorbed pump power for one of the beams. The threshold value was evaluated to 820 mW.*

# 7 Monolithic, single mode Nd-laser with a grating outcoupler

With the results, and more important, methods for building and aligning two trial cavities, a monolithic setup was built. The Bragg grating was still used as outcoupler, with the modification of making a single-unit cavity. In other words, the grating was glued to the Nd:$GdVO_4$ using the same kind of PDMS that held the incoupler and gain medium together. Here efficient output was desired, as well as single mode operation and hopefully a low $M^2$ value.

## 7.1 Experimental setup and measurements

In this setup there was only one cavity piece to work with; the coated incoupling lens (mirror) glued to the gain medium which in turn was glued to the oucoupling Bragg grating using PDMS, creating a monolithic device of physical length 8 mm. A schematic view of this can be seen in Fig.7.1. As in the previous section, two alignment lasers had to be used; A HeNe for alignment of the incoupler and one at 1066 nm for alignment of the grating. As always, the pump was blocked and the output beams were focused into a spectrum analyzer as well as a power meter to get the desired data. To determine the polarization of the beams, a glan polarizer was used. Furthermore, using the knife-edge technique discussed in section 2.1.1.1, $M^2$ and the cavity beam waist $W_0$ were determined.

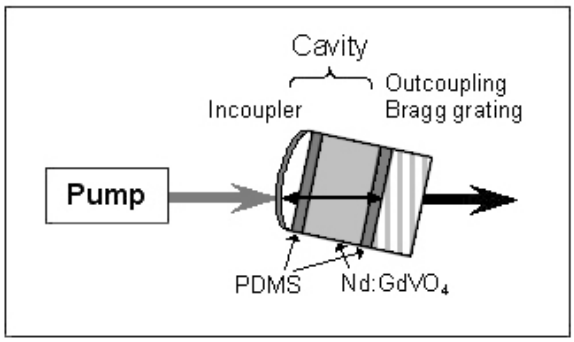


***Figure 7.1.*** *View of the setup. The incoupler is a HR@1064 nm, HT@808 nm coated lens (mirror), glued to the gain medium by a very thin layer of PDMS. The outcoupling Bragg grating is also glued to the gain medium.*

### 7.1.1 WinLase cavity simulation

Even though not much had changed from section 6, a WinLase simulation for this new setup was made (Fig.7.2). Having one less degree of freedom since the distance between the gain medium and outcoupler was now fixed, it was of interest to check the stability of the cavity. The single-unit cavity proved stable according to WinLase. The pump size was to be of equal magnitude as the gaussian mode size within the gain medium, which was found to be $\sim$35 $\mu$m. The pump focus thus agreed with the restriction, and no changes had to be made.

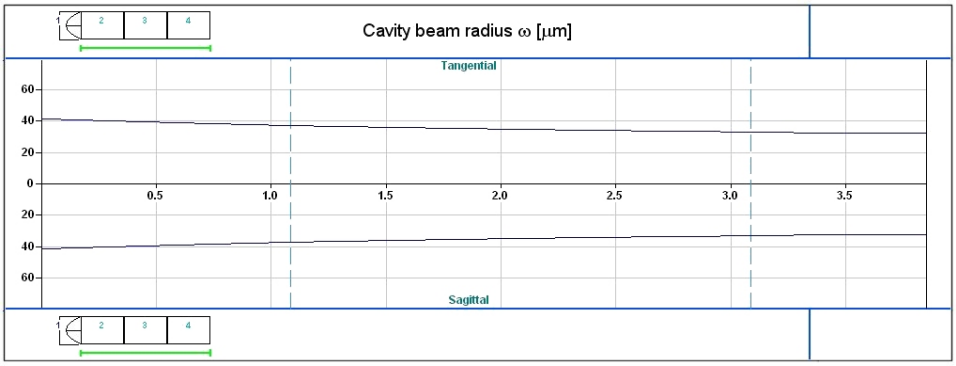


***Figure 7.2.*** *WinLase model of the setup. The gaussian mode size within the gain medium is around 35$\mu$m.*

## 7.2 Results

Aligning the cavity was much harder for this setup compared to the trial setups, since all components were glued together. However, after much work, the cavity was properly aligned and output beams were showing. Like before, four beams were present. This time however, there should have been 9 beams, two from each interface and one from the entire roundtrip. The interface reflections are, according to Eq.3.15, 0.09%, 3%, 3% and 0.04% (times two), whilst the roundtrip outcoupling was 0.5%. Hence, the four 3% beams are dominant and the other 6 ouputs can be neglected since they were comparatively too weak to be noticed. A depiction of the reflection outputs is seen in Fig.7.3. The four beams had roughly the same intensity and were diverging due to diffraction caused by the small focus. Also, the beams were all $\sigma$-polarized.

### 7.2.1 Threshold value of the setup

The output power of the four beams as a function of the, by the gain medium, absorbed power was measured and the results are seen in Fig.7.4 through

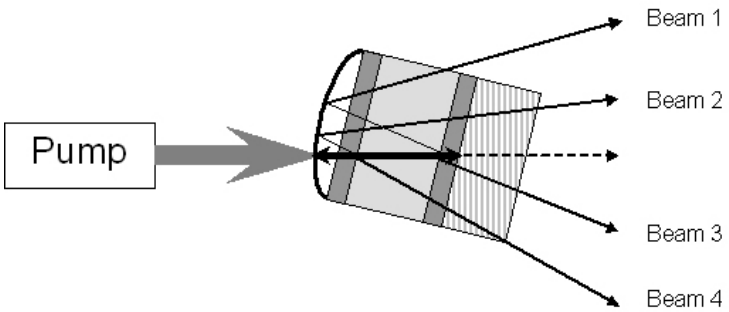


***Figure 7.3.*** *The four output beams originating from interface reflections within the cavity.*

7.7. It should be noted from the figures that the laser power drops at high

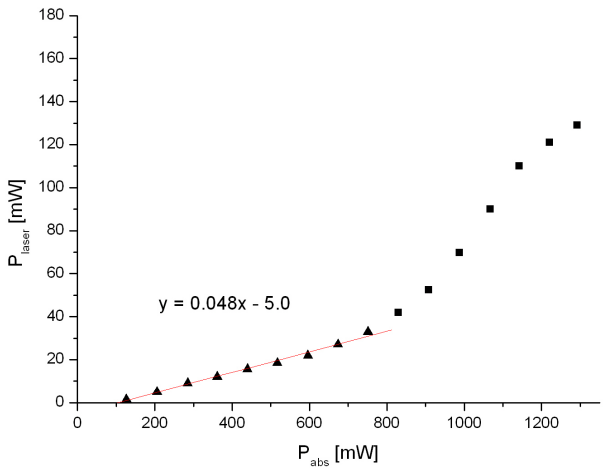


***Figure 7.4.*** *Beam 1.*

pump powers. The laser outputs showed decreased stability with increased pump, with slow variations due to thermal effects. Higher pump powers of course leads to a higher temperature of the gain medium as well as the PDMS surrounding it. This will lead to an expansion the Nd:$GdVO_4$, and the silicone which will have an overall unknown reaction to the expansion and the high temperature. This instability was not seen at lower pump powers, i.e. lower temperatures which is why the lower powers were studied further. The four threshold values for the output beams were 104 mW, 100 mW, 164 mW and 110 mW respectively. The thresholds should of course

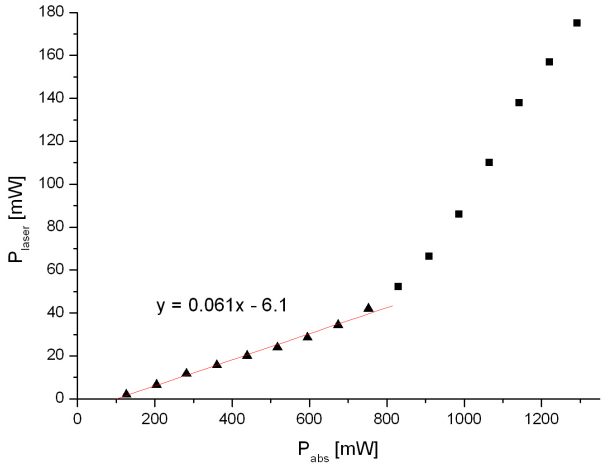


***Figure 7.5.*** *Beam 2.*

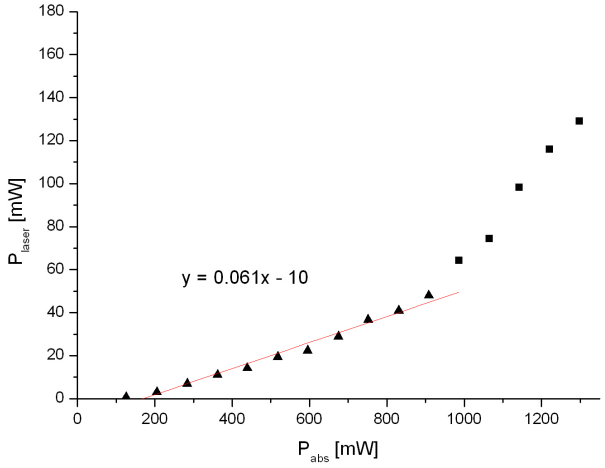


***Figure 7.6.*** *Beam 3.*

coincide, but measurement errors separated them. The slope efficiencies $\eta_{eff}$ were not impressive, ranging from 0.04 to 0.061. Again, the output was not optimal. Furthermore, the same behaviour as in section 6 is also seen here, with intersections between lower and higher slope efficiency regions. Like before, this can probably be explained by the excitation of higher transverse modes.

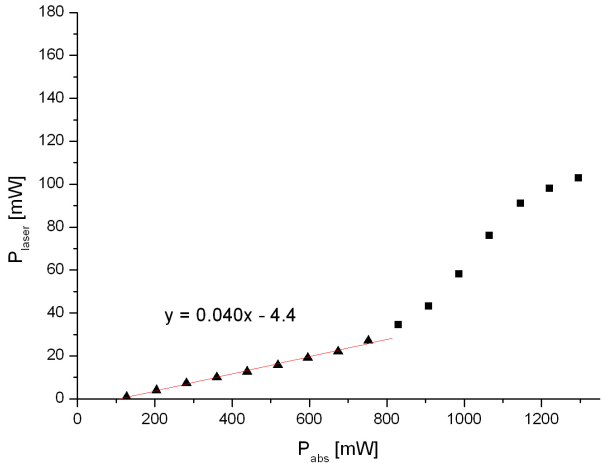


***Figure 7.7.*** *Beam 4.*

It was also interesting to study the sum of all beam powers. One of the reasons for the fairly low output is of course that it was divided into four beams instead of one. If gathering their total effect, one could attain a quite high power output. The power sum is seen in Fig.7.8, with a threshold of 117 mW and a maximum laser power of 550 mW for 1300 mW of absorbed pump. Compared to the maximum output of 100-164 mW for an individual beam, this is a big improvement.

### 7.2.2 Beam quality

The desired laser beams are single longitudinal mode operated, and as close to gaussian as possible. The achieved beams however, were of less quality. Using the knife edge technique on the beam, the beam divergence, waist as well as the $M^2$ value could be determined.

The value found was $M^2 \approx 2.4$ for low pump powers. $M^2 = 1$ corresponds to a pure gaussian beam, which was obviously not the case here. The high value implies higher transverse modes which, however undesired, nevertheless were present. Furthermore, the whole divergence angle was determined to $\theta = 52$ mrad, or given in degrees $\theta = 2.98°$. The beam waist within the cavity was found to be 63 $\mu$m, which gives a gaussian beam waist of (divide by M) just over 40 $\mu$m confirming the measurements.

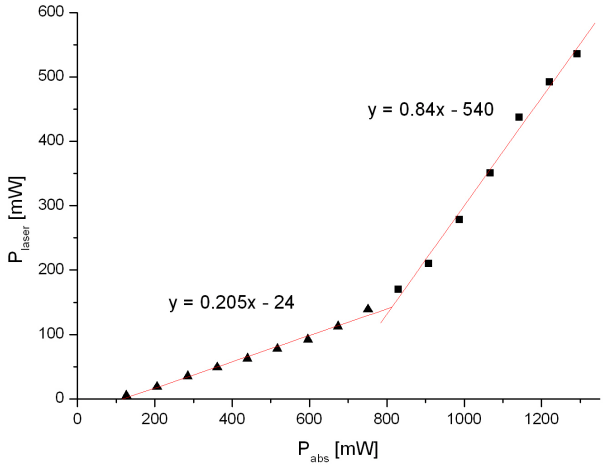


***Figure 7.8.*** *The sum of the laser power of the four output beams.*

### 7.2.3 Fabry-Pérot measurements

In order to attain more precise values of the mode separation, as well as determine how to achieve single mode operation, one of the output beams was coupled into a Fabry-Pérot interferometer.

#### 7.2.3.1 Temperature dependence

When heated, the Nd:$GdVO_4$ crystal will expand. This will in turn alter the cavity length and thus affect the oscillating modes. To determine the expansion of the crystal, the frequency shift of the mode with changing temperature was studied, and the results can be seen in Fig.7.9. 24°C could be set as the frequency zero level, since only the frequency shift was of importance here. The pump power was held constant at $\sim$ 290 mW, a little above the cavity threshold. Thus, a temperature change $\Delta T$ of 1°C corresponds to a mode frequency change $\Delta\nu$ of -2.99 GHz, or a wavelength change of 0.01 nm (frequency change and wavelength change have opposite sign). Hence, the frequency drops as the cavity expands.

**Thermal expansion**

The oscillating modes in the cavity will be standing waves so that $\eta L = N\lambda/2$ where $\eta$ is the refractive index, $L$ is the cavity length and $\lambda$ is the wavelength. $N$ is the number (integer) of half wavelengths in the standing wave, where $N = 1$ corresponds to half a wavelength, $N = 2$ one wavelength

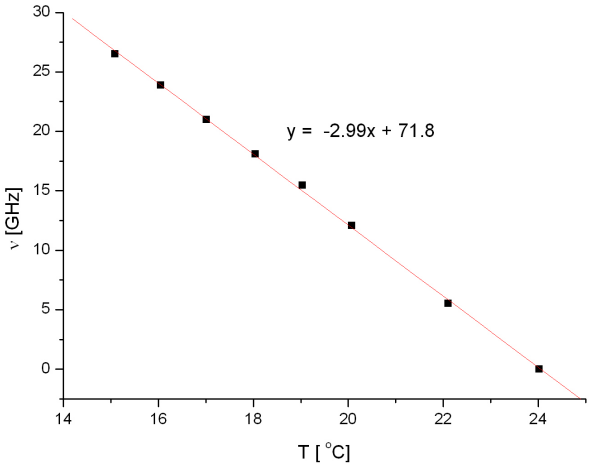


***Figure 7.9.*** *The mode frequency vs. the crystal temperature. Here* $24°C$ *was set as the frequency zero level.*

and so on. Obviously, a cavity length change will induce a laser wavelength change. If assuming that the refractive index $\eta$ also is affected, one can derive

$$\frac{\Delta\lambda}{\lambda} = \frac{\Delta L}{L} + \frac{\Delta\eta}{\eta}, \tag{7.1}$$

which will, when looking at the temperature change, yield

$$\frac{\Delta\lambda}{\Delta T}\frac{1}{\lambda} = \frac{\Delta L}{\Delta T}\frac{1}{L} + \frac{\Delta\eta}{\Delta T}\frac{1}{\eta}, \tag{7.2}$$

The first term to the right of the equality sign is again identified as the thermal expansion coefficient $\alpha_T = \Delta L/L\Delta T$. Thus, using $\Delta\lambda/\lambda\Delta T = -\Delta\nu/\nu\Delta T$

$$-\frac{\Delta\nu}{\nu\Delta T} = \alpha_T + \frac{\Delta\eta}{\Delta T}\frac{1}{\eta} = \alpha_{T,eff}, \tag{7.3}$$

where $d\eta/dT$ ($\Delta\eta/\Delta T$) is the *thermo-optic coefficient*. We define the *effective thermal expansion coefficient* $\alpha_{T,eff}$ as the sum of $\alpha_T$ and $d\eta/dT \cdot 1/\eta$. Since the Bragg wavelength $\lambda_B$ is given by Eq.3.8: $\lambda_B = 2\eta\Lambda$ (for $\theta = 0$), equivalent derivation as for $N\lambda = \eta L$ will yield the same relation as above (Eq.7.3). Hence, the equation can also be used to calculate the effective thermal expansion coefficient for the grating. Further derivation using $-\Delta\nu/\nu\Delta T = -\Delta L/L\Delta T$ yields

$$\frac{\Delta L}{\Delta T} = \alpha_{T,eff} L, \tag{7.4}$$

Here $\Delta\nu = -2.99$ GHz, $L = 6.4$ mm and $\nu = 281$ THz will be the center values. The effective thermal expansion coefficient $\alpha_{T,eff}$ of the entire cavity will be $11 \cdot 10^{-6}/°\text{C}$, and by using Eq.7.4 the cavity length expansion $\Delta L/\Delta T$ will equal 68 nm/°C. The change in cavity length is mainly caused by the expansion of the absorbing crystal, but also by expansion of the Bragg grating as well as the lens due to the temperature change. Note that this value may not be the exact cavity length change. It should be though of as the cavity length change corresponding to a certain frequency change, rather than the physical cavity expansion of 68 nm/°C.

Since we are dealing with a monolithic piece, we have to look at the thermal expansion when adding several components. Eq.7.4 has to be rewritten into

$$\alpha_{T,eff} = -\frac{\Delta\nu}{\nu\Delta T} = \frac{1}{L}\sum_i (\alpha_{T,i} + \frac{d\eta_i}{dT}\cdot\frac{1}{\eta_i})\eta_i L_i, \tag{7.5}$$

where the quantities labeled $i$ correspond to the different materials of the cavity. $L$ is still the total optical length of the setup, 6.4 mm.

### Thermal expansion of the Bragg grating

To determine how much the Bragg grating expanded, a whole mode cycle was studied. The grating expansion was slightly slower than the movement of the modes, $|v_{mode}| > |v_{Bragg}|$, which is shown in Fig.7.10. Here "velocity" is referred to as the frequency drift per degree Celcius. Half a mode cycle,

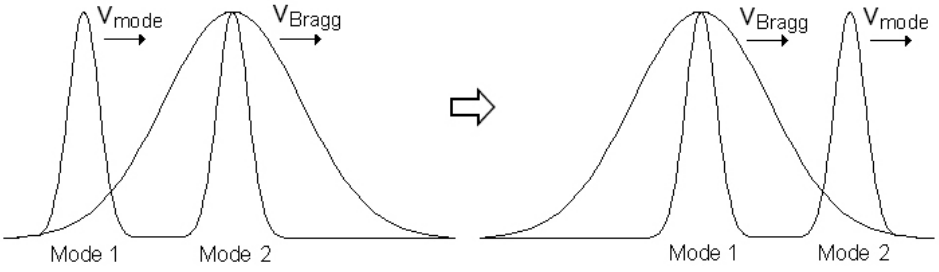


***Figure 7.10.*** *The Bragg reflection peak moves with velocity $v_{Bragg}$, whilst the cavity modes move with velocity $v_{mode}$.*

i.e the growth and death of one mode depicted in Fig.7.11, correspond to a frequency change of 23.4 GHz which is the mode separation according to Eq.2.14. The modes changed almost one cycle, approximated to 0.8 cycles, over a temperature change of 55°C, leading to a velocity change $\Delta v = 0.8 \cdot 23.4$ GHz/55°C= 0.34 GHz/°C. This is thus the offset from the velocity of the modes $v_{mode}$, calculated to -2.99 GHz/°C earlier. The grating thus expands with the velocity $v_{mode} + \Delta v = -2.65$ GHz/°C or given in units

of length, 0.01 nm/°C. The wavelength change due to thermal expansion has been experimented on and calculated by others as well, and a drift of $0.01nm/°C$ seems to be accurate for this type of setup [14]. The effective thermal expansion coefficient of the bulk grating could be determined by Eq.7.3, with the result $\alpha_{T,eff} = 9.4 \cdot 10^{-6}$/°C.

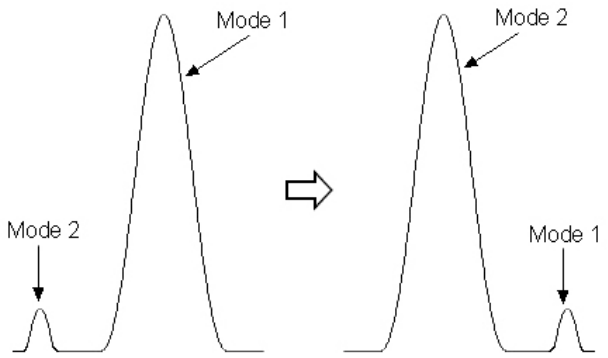


***Figure 7.11.*** *Half a mode cycle; The dying from the peak value of one single mode whilst a new one grows to it's peak value.*

To carry out the theoretical comparison with the experimental value, the thermal expansion coefficients and thermo-optic coefficients from table 3.1 were used. When neglecting the thicknesses of the PDMS layers, a change of 1°C yields an expansion of the monolithic piece of (Eq.7.5) 1.517·1.08 mm·(7.1+2.1/1.517)·$10^{-6}$+2·2 mm·(7.3+4.7/2)·$10^{-6}$=52 nm per degree Celcius. Here the contribution of the Bragg grating is not included. Since the effective grating length is $L_{eff} = \sqrt{R_{max}}/2\kappa$ (Eq.3.14), it will not follow the thermal expansion relations derived here. In principal the expansion of the grating could be derived from Eq.3.14, however omitted in this thesis.

The calculated value of 52 nm/°C is in slightly off the attained value of 68 nm/°C. Furthermore, the theoretical $\alpha_{T,eff}$ must, according to Eq.7.5, be 52 nm/°C divided by the total cavity length of 6.4 mm, resulting in $\alpha_{T,eff} = 8 \cdot 10^{-6}$/°C, compared to the experimental value of $11 \cdot 10^{-6}$/°C. Again, if including the contribution from the grating the theoretical value would be larger and closer to the experimental one.

#### 7.2.3.2 Transverse modes

The Fabry-Pérot scanning showed that the output was operating in multi transverse mode, depicted in Fig.7.12. The figure was attained at $P_{pump}$ = 480 mW and a crystal temperature of 27°C, and shows single longitudinal

modes, with side bands identified as higher transverse modes. From the

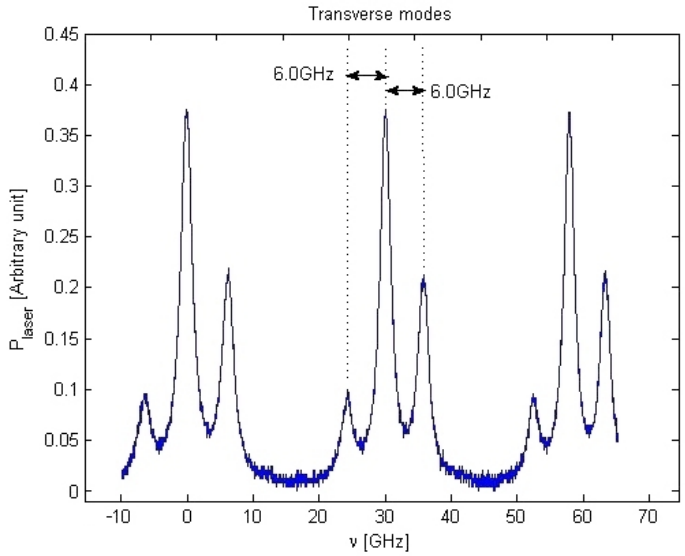


***Figure 7.12.*** *Fabry-Pérot scanning of the transverse modes, which are separated by 6 GHz.* $P_{pump} = 1600\ mW$ *the crystal temperature is* $27°\,C$.

figure, it is found that the transverse mode separation is 6 GHz. The theoretical frequency separation $\Delta\nu_{qnm}$ between the transverse modes in the cavity is given by [8]

$$\Delta\nu_{qnm} = \frac{c}{2L}(\Delta q + (\Delta n + \Delta m)\frac{cos^{-1}(\pm\sqrt{|g_1 g_2|})}{\pi}), \tag{7.6}$$

where $g_1 = 1 - L/R_1$ and $g_2 = 1 - L/R_2$ determine the cavity stability for a cavity with an incoupling ROC $R_1$ and outcoupling ROC $R_2$. Here $R_1 = 6.2$ mm, and since the outcoupler (grating) is plane, $R_2 = \infty$. The $q, n$ and $m$ determine the order of the transverse mode (all equal to zero correspond to the first, gaussian mode $TEM_{00}$). We are interested in the first side bands, i.e. equal $q$-value and a change in either $n$ or $m$ for witch the other one remains the same. Thus, $\Delta q = 0$ and $\Delta n + \Delta m = 1$. With an optical cavity length $L$ of 6.4 mm, the transverse mode separation is roughly 10 GHz, which agrees with the experimental value in order of magnitude. The sidebands are hence identified as higher transverse modes, which explains the $M^2$ value of 2.4. Since two higher order transverse modes are present in the figure, one of the peaks must be $TEM_{00}$, the other $TEM_{01}$ or $TEM_{10}$ and finally the third peak which must be $TEM_{11}$, $TEM_{02}$ or $TEM_{20}$.

#### 7.2.3.3 Longitudinal modes

It was shown in the previous paragraph that the laser output was operating in single longitudinal mode. This was not always the case however. When changing the pump power or the crystal temperature, multi longitudinal mode operation occured. Higher crystal temperature meant lower pump power to still have single mode operation. Fig.7.13 shows two longitudinal modes oscillating, each with higher transversal side modes. The data was attained for $P_{abs}$ = 830 mW and the crystal temperature 45°C. Changing

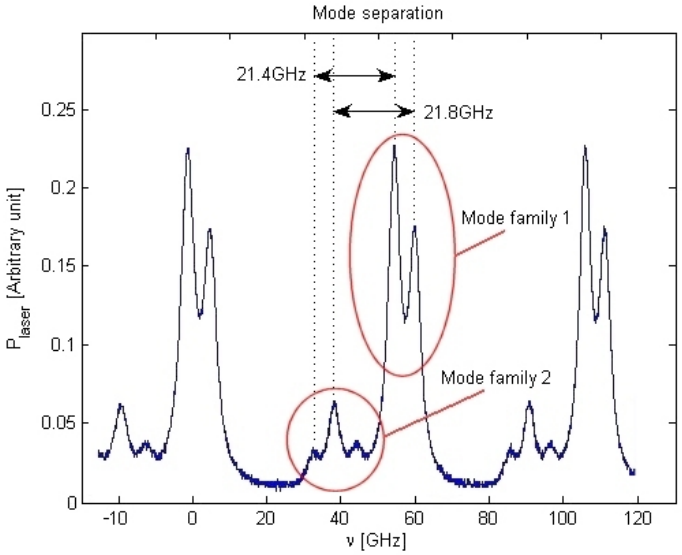


***Figure 7.13.*** *Fabry-Pérot scanning of two longitudinal modes, separated by slightly under 22 GHz.*

the temperature or pump power translated into one of the longitudinal modes growing while the other one was dying. The sidebands are transverse modes as discussed previously. It can be seen that the longitudinal mode separation is just under 22 GHz. This is equivalent to a cavity length of just below 7 mm, compared to the cavity's actual optical path length of 6.4 mm (when neglecting the PDMS glue). The difference is probably due to the human error in measuring, mainly the Fabry-Pérot cavity length which was hard to measure as well as the monolithic cavity length. Since the incoupler was very curved, pumping just slightly off the center leads to some difference in the cavity length and thus increases the inaccuracy of the measurements.

**Frequency tuning**

While carrying out the measurements, it was noticed that single longitudinal mode operation was fairly easy to achieve, by adjusting the pump power and/or crystal temperature. For temperatures spanning from 15°C to 50°C single mode operation was possible (for maximum pump powers of 2900 mW through 580 mW respectively). This temperature span is equivalent to a shift of around 105 GHz or 0.4 nm, allowing for some tuning of the laser.

The frequency shift was very smooth and stable and once the temperature had stabilized, the modes were also stable. Hence, with the drawback of quite low output powers, the setup produced a stable, narrow and slightly tunable laser.

# 8 Monolithic, single mode Nd-laser with a grating incoupler

The goal of achieving a lasing monolithic laser cavity was reached for the setup described in section 7. The results however, were not very satisfying, not least due to the four output beams instead of one. In order to attain only one output beam (or at least one superior output), the setup was modified, the aim being a higher quality (lower $M^2$ value), single output.

## 8.1 Experimental setup and measurements

The monolithic piece described in the previous section was still used, but flipped to let the Bragg grating work as incoupler instead of outcoupler. The former incoupler was switched to a similar lens but with a different coating of reflectivity 82% at 1064 nm. Now being the outcoupler, it allowed larger cavity output closer to the losses and thus hopefully improving the output. The new monolithic cavity can be seen in Fig.8.1. This time, only a HeNe alignment laser was used to adjust the cavity. After aligning the outcoupler, the "trial and error" approach was used to also align the grating, a method proving very efficient. As before, after filtering the pump, a lens was used to focus the beam into a power meter as well as a fiber coupled to a spectrum analyzer. Using a glan polarizer, the beam polarization could be determined.

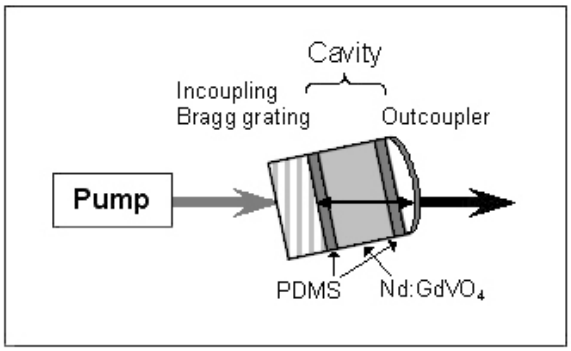


***Figure 8.1.*** *View of the setup. The incoupler is a Bragg grating, glued to the gain medium by a very thin layer of PDMS. The outcoupler, a R=82% at 1064 nm coated lens (mirror), is also glued to the gain medium.*

### 8.1.1 WinLase cavity simulation

A model of the new setup was made, and is seen in Fig.8.2. It is very similar to the previous simulation, with a mode size of around $35\mu m$ here as well. Furthermore, the monolithic setup proved stable.

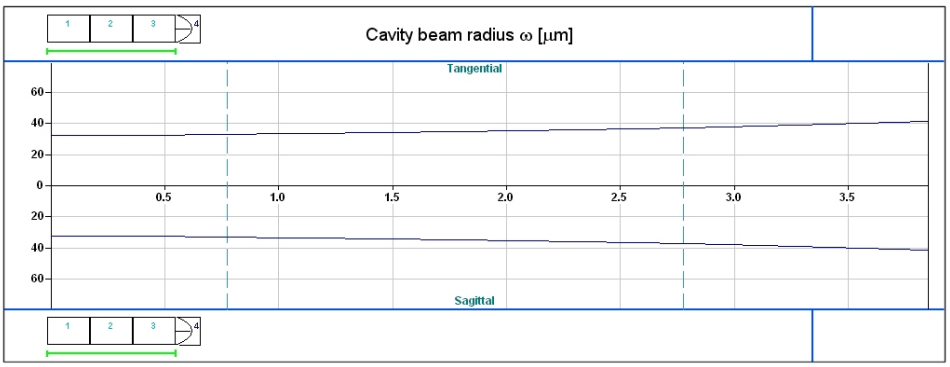


***Figure 8.2.*** *WinLase model of the setup. The gaussian mode size within the gain medium is around* $35\mu m$.

## 8.2 Results

After alignment, the cavity was lasing. Although three output beams were present, one of them was dominant and of much larger intensity than the other ones which were hardly visible. This is the cavity resonant beam at 12% outcoupling compared to the reflections at up to no more than 3% output. The two other, slightly visible beams were the 3% back and forth reflections from the PDMS-Nd:$GdVO_4$ interface (should be four of those beams, but the other two must have been coinciding with the visible two), depicted in Fig.8.3. The beam was $\sigma$-polarized and, like before, diverging due to diffraction caused by the small beam waist within the cavity.

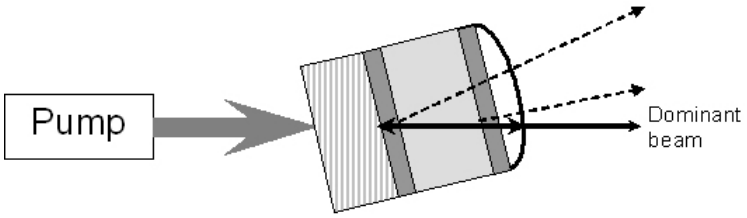


***Figure 8.3.*** *The three output beams. The dominant one is the cavity roundtrip outcoupling, and the other two originate from interface reflections within the cavity*

### 8.2.1 Threshold value of the setup

The output power of the main laser beam was studied and the threshold value of the cavity was calculated. The laser output vs. the absorbed pump power is seen in Fig.8.4. The threshold value is found to be ∼263 mW of

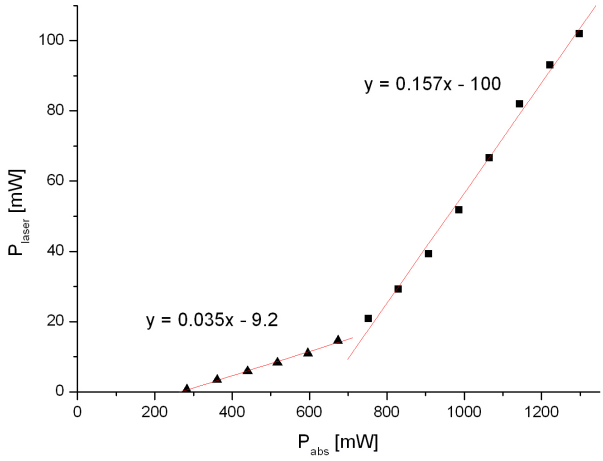


***Figure 8.4.*** *Laser power vs. absorbed power. The threshold value is roughly 263 mW.*

absorbed power. Two slope efficiencies were calculated, one for low pump powers and one for high, with the results $\eta_{eff} = 0.035$ and 0.157 respectively. The setup showed larger stability at higher temperatures compared to the setup in the previous section 7. Like in the previous sections, the slope efficiency suddenly starts to increase yielding larger power output. Again, this is thought to be the point where higher transverse modes start lasing.

#### 8.2.1.1 Comparison of the threshold values

Comparing the threshold value of this setup, 263 mW, with the average threshold in the previous setup (section 7) found to be ∼120 mW, the ratio is roughly 2.2. The ratio of the two thresholds given by Eq.4.1 will simply be $\delta_1/\delta_2$. If assumed a 1% scattering loss together with the Fresnel reflection roundtrip loss of 11.2%, $\delta_1 = 11.2+1+0.5 = 12.7\%$ and $\delta_2 = 11.2+1+12 = 24.2\%$. Their ratio is around 2 compared to the threshold ratio of 2.2, the two values thus agreeing.

Further comparison with this threshold and the one found in section 6 of 820 mW yields a ratio of around 3. The two $\delta$ are $28 + 1 + 0.5 = 29.5\%$ and 24.2% respectively, yielding a ratio of 1.2. Obviously the two values are not coinciding, probably due to measurement errors.

### 8.2.2 Laser spectrum

The peak wavelength of the laser was found to be 1066.1 nm according to the spectrum in Fig.8.5. Here the operation is single-single mode, i.e. single longitudinal and transverse mode. The FWHM is determined to ∼0.06 nm. This is however the resolution of the spectrum analyzer, so the attained value should only be looked at as an upper limit of the full width half maximum, and not the exact value.

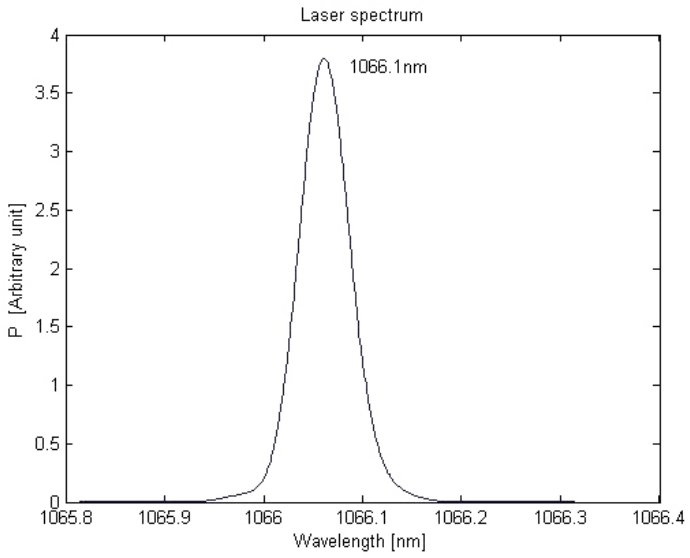


***Figure 8.5.*** *Laser spectrum showing the peak emission at 1066.1 nm.*

### 8.2.3 Beam quality

Using the knife-edge technique yielded $M^2 = 1.02 \approx 1$ for single-single mode operation (here, $P_{abs} = 350$ mW and $T = 17°C$) which is identified as a gaussian beam. The divergence angle $\theta/2$ was roughly 10 mrad. Since the beam exited the cavity through a focusing lens thus altering the angle, WinLase was used to trace the beam backwards through the lens and into the cavity. The beam waist $W_0$ was determined to 35 $\mu$m in accordance with the pump size. Similarly, multi transverse mode operation ($P_{abs} = 1300$ mW and T=17°C) yielded an $M^2 = 3.0$. The measured divergence angle was $\theta/2 = 0.015$, meaning a gaussian angle of (divide by M) 9 mrad very close to the measured gaussian value for lower pump powers. Thus the beam waist within the cavity for transverse mode operation should equal the gaussian waist multiplied by M, in this case 35 $\mu$m$\cdot\sqrt{3} = 61$ $\mu$m.

It was hence found that for single-single mode operation (discussed in more detail below) the $M^2$ value was actually 1 as is should be.

### 8.2.4 Fabry-Pérot measurements

In order to study the mode separation, as well as determine temperature intervals with single mode operation, the output beam was coupled into a Fabry-Pérot interferometer.

#### 8.2.4.1 Temperature dependence

The expansion of the cavity and the frequency shift of the oscillating modes with changing temperature was studied for this setup as well, results seen in Fig.8.6. 25°C was set as the frequency zero level, since only the frequency shift was of importance. The pump power was held constant at around 430 mW. Thus, a temperature change $\Delta T$ of 1°C corresponds to a frequency

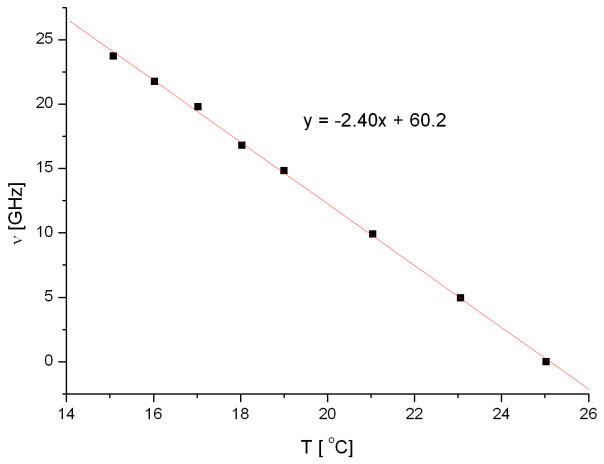


***Figure 8.6.*** *The mode frequency vs. the crystal temperature. Here 25° C was set as the frequency zero level.*

change $\Delta\nu$ of -2.40 GHz, or a wavelength change $\Delta\lambda$ of 0.009 nm.

#### Thermal expansion

With $\nu = 281$ THz, the effective thermal expansion coefficient $\alpha_{T,eff}$ is found by Eq.7.3 from the previous section, yielding the result $9 \cdot 10^{-6}$/°C. Using Eq.7.4, with L=6.4 mm, the cavity length change $\Delta L/\Delta T$ will equal 55 nm/°C. The reason for the disagreement with the last setup ($\alpha_{T,eff} =$

$11{\cdot}10^{-6}/°\mathrm{C}$) is probably due to the change in pump and cavity mode overlap when flipping the cavity, as well as less efficient cooling of this setup due to PDMS residue surrounding the crystal. In addition, the temperature of the cooler may not be the same as the actual temperature of the crystal, leading to disagreement. Furthermore, the temperature within the monolithic piece is probably not evenly distributed throughout the piece as assumed here. It is likely that the temperature of the crystal is higher than that of the lens and Bragg grating.

Finally, the attained effective expansion coefficients of this section and the previous, were values of 9 and $11{\cdot}10^{-6}/°\mathrm{C}$ respectively, with the theoretical value of $8 \cdot 10^{-6}/°\mathrm{C}$. Again, the disagreement is probably due to the omission of the grating expansion in the theoretical calculation, which otherwise would have yielded a larger value closer to the experimental ones.

#### 8.2.4.2 Transverse modes

Recalling the previous section, it was found that the transverse mode separation is roughly 10 GHz for the setup. Even though the cavity of this section is mirrored compared to the previous one, that doesn't affect the transverse mode separation. Looking at the case T=17°C and $P_{abs}$ = 440 mW, the output looks like that in Fig.8.7. The transverse mode separation

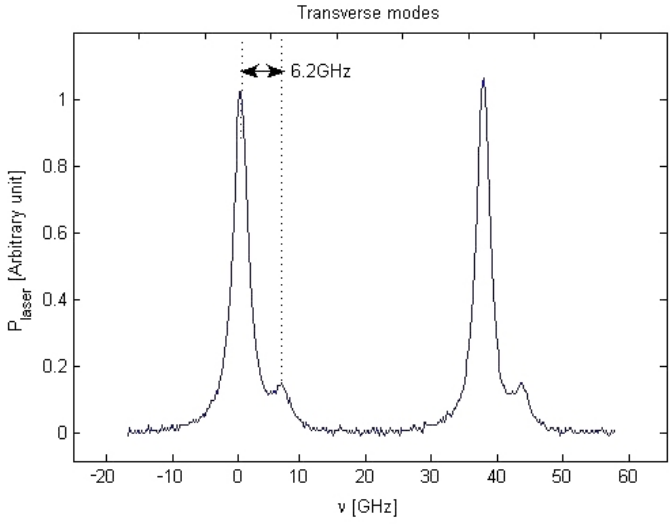


***Figure 8.7.*** *Single longitudinal mode operation with one higher transverse mode.*

is 6.2 GHz, more or less equal to that of the previous setup. Hence, the sideband is identified as a higher transverse mode.

#### 8.2.4.3 Longitudinal modes

Different from the setup described before in section 7, multi longitudinal mode operation was possible to combine with single transverse mode, as seen in Fig.8.8. Here the crystal temperature was set to 15°C and the absorbed pump power was 430 mW. The separation $\Delta\nu$ is 22.9 GHz, corresponding to an optical cavity length of a bit under 6.6 mm, agreeing with the actual length of ∼6.4 mm.

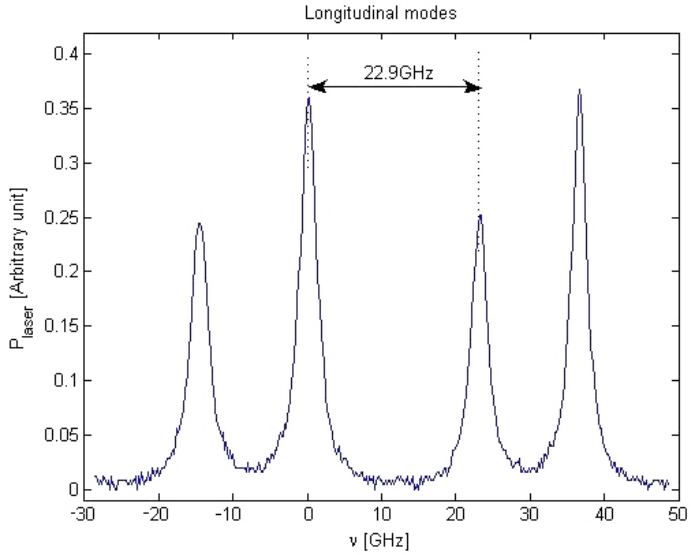


***Figure 8.8.*** *Two longitudinal modes oscillating, separated by 22.9 GHz.*

#### 8.2.4.4 Single-single mode operation

When scanning the laser output with the Fabry-Pérot, it was found that it was possible to achieve single transverse as well as longitudinal mode operation by adjusting the crystal temperature and pump power. Fig.8.9 was obtained for an absorbed pump power of 830 mW and a Nd:$GdVO_4$ temperature of 27°C. The FWHM was determined to 0.36 GHz or 1.4 pm, hence being the upper limit of the bandwidth, limited by the Fabry-Pérot finesse of 8 from Eq.2.16.

**Frequency tuning**

The modes were studied at different pump powers, and by changing the crystal temperature intervals were found where there was single transverse mode

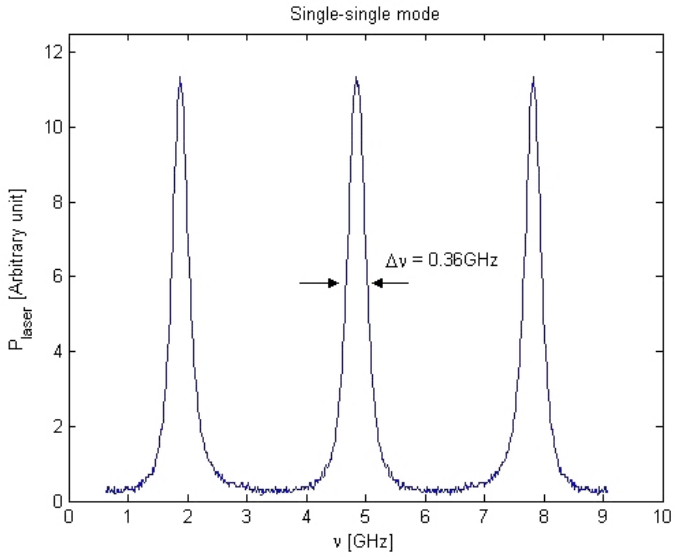


***Figure 8.9.*** *Fabry-Pérot scanning showing single transverse and longitudinal mode operation.*

operation, single longitudinal mode operation as well as both single longitudinal and transverse mode operation. The temperature interval looked at ranged from $15°C - 70°$C, and the result is shown in Fig.8.10. As can be seen in the figure, both single transverse and single longitudinal mode operation is possible. The frequency is also shown as the second y-axis, where 15°C is set as the frequency zero level, the only interest being the shift, not the actual value. The figure tells us that higher transverse modes start to appear at around 800 mW of absorbed power (they appear for lower powers as well, but only for high temperatures). When studying the threshold value, it was noted that there was a sudden jump where the slope of the laser power started to increase, for this setup occurring at around 800 mW according to Fig.8.4. It was suggested that this was the result of higher order transverse modes starting to lase, which apparently seems to have been the correct assumption.

Further study of the intervals at the absorbed pump power of 830 mW gives an idea of the tunability of the laser. The overlapping interval with single-single mode operation spans from $27°C - 62°$C. This temperature range corresponds to a frequency shift of 84 GHz or a wavelength shift of just over 0.3 nm. This is thus the tunability (for that pump power) of the laser produced with the requirement of single-single mode operation. The value of course differs with other pump powers, but 0.3 nm is an estimate of the tunability.

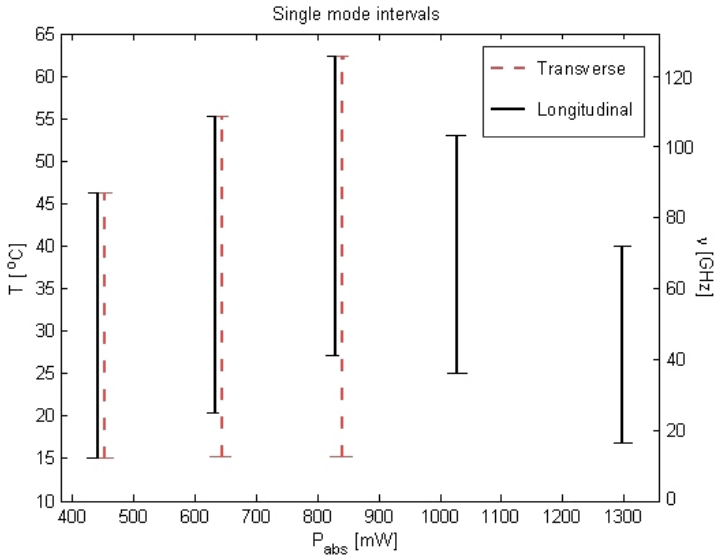


***Figure 8.10.*** *Temperature and frequency intervalls with single mode operation. The full line intervalls represent single longitudinal mode, whereas the dashed intervalls are single transverse mode operation.*

### Stability

A stable laser output is always strived for. For this setup, both power stability with changing crystal temperature as well as frequency stability over time was desired. Looking at the temperature interval for single-single mode associated with $P_{abs} \approx 830$ mW, it ranges from $27 - 62$°C. When measuring the laser power for this entire range, it was noted that the power dropped when increasing the temperature when not changing the cavity. If the alignment was optimized for single-single mode however, the output power proved stable.

The power and frequency stability over time was also investigated. For single-single mode oscillation ($P_{abs} = 830$ mW and crystal temperature 27°C) the mode frequency was studied. After stopping the scanning, the output from the Fabry-Pérot was studied through the oscilloscpe. The power at 50% of the maximum value (where power changes are most visible due to the largest slope) was studied. A power change is the result of the mode frequency moving away from the peak of the interferometer, and can thus be used as a measure of the frequency change. The oscilloscope created a histogram of the power for some different time spans. For a 10 s measurement, the standard deviation $\sigma_{sdv}$ was found to be 4.2%. Looking at the plot in Fig.8.9, the frequencies around half the maximum, $50\% \pm 4.2\%$ were found, and their separation was determined to 66 MHz. Hence, the stability

over 10 s was around 66 MHz. Equivalently, a 100 s time interval resulted in $\sigma_{sdv} = 18\%$ or 107 MHz. It should be noted that the deviations are upper limits, since it is impossible to say if they are the result of the laser or the Fabry-Pérot being unstable.

The power stability over time was easier to calculate. The detector was simply placed in front of the interferometer, and equivalent to the frequency stability, a histogram of the power was created. This time however, the histogram directly represented the power fluctuation and the 10 s and 100 s fluctuations were found to be 1.5% and 3.6% respectively.

As before, the frequency shift was very stable and smooth, and once the temperature had stabilized, the operating modes were also stable. Once again the setup produced a narrow, stable and continuously tunable laser.

# 9 Discussion

To summarize the most important results, it was found possible to construct a single-single mode operated 1.06 $\mu$m laser, using a monolithic Nd:$GdVO_4$ cavity, frequency-locked by a volume Bragg grating. The aim for an equivalent setup, using Nd:glass instead was however not reached.

After studying the results obtained from the spectroscopic measurements done on the two gain media, it is possible to explain why the laser output for some of the Nd:$GdVO_4$ setups was $\sigma$-polarized, and not $\pi$. It was found that the emission crossection was more than 2 times higher than that for $\sigma$. However, the emission peak is at $\sim$1064 nm for $\pi$ and at $\sim$1066 nm for $\sigma$. Thus, for all setups when the Bragg grating was used as one cavity mirror, the $\sigma$-polarization was favored and the laser was polarized accordingly.

For the monolithic setups high power pumping was not possible for $TEM_{00}$ operation. For the setup discussed in section 7, $TEM_{00}$ operation was never attained. I think this is a result from too poor overlap with the pump mode and the gaussian mode within the cavity. For one, the pump had a $M^2$ value of around 40, which decreases the gaussian mode overlap. Moreover, the small pump focus was quite divergent leading to poor overlap at the ends of the gain medium in which the gaussian mode was not as divergent.

The reason for the fairly large tunability of the monolitchic setups comes from the fact that the Bragg reflection peak expands with almost the same velocity as the cavity modes when changing the temperature. A large difference between $v_{Bragg}$ and $v_{mode}$ would very quickly lead to poor overlap between the cavity frequency and the narrow reflection band of the grating. Hence, the lasing would cease rapidly and almost no tuning would be possible. However, since the thermal expansion coefficients are very similar for the crystal and grating, the grating reflection peak follows the mode frequency change, allowing lasing in a quite large interval. The result is continuous tunability over a quite large interval.

## 9.1 Conclusions

Nd:glass is a very efficient and in reality very good laser gain material, even though it proved insufficent for this thesis project. For larger, non-monolithic setups it shows high performance. However, tiny monolithic cavities demand small pump focuses when overlap with only the gaussian mode is desired. This fact prevents glass hosts (hosts with poor thermal properties) from working efficiently and with high performance in a small monolithic setup.

It is possible, and fairly easy to construct and align a monolithic setup. With the attained stability and tunability, I have showed that the laser can

also be high quality, quite efficient and narrowbanded. It is my belief that the quite low power output can be improved, by optimizing the pump and cavity mode overlap. Furthermore, the gain crystal can be pumped harder than 3.3 W to achieve a more powerful output.

## 9.2 Future work

In this thesis, it was shown that it is possible to build a monolithic laser cavity. Furthermore, it was frequency-locked and single-single mode operated which produced a narrow bandwidth output laser. The first steps towards an effective and high quality monolithic laser are thus taken. There are however many improvements and elaborations of the design which can be made.

### 9.2.1 Material improvements

The Nd:glass material proved insufficient for this project. The simpler setups, on the way to the monolithic laser, did not lase before damaging the glass gain medium. The end surfaces of the glass pieces were not coated in anyway, which of course led to higher losses within the cavity. Antireflection coatings for the laser wavelength would have lowered the threshold, and maybe enabled lasing for the non-monolithic cavities. For a monolithic setup, one could have applied a special thin film antireflection coating working despite higher refractive index materials on both sides of the coating instead of one as is the case for normal coatings. The use of this type of coating could of course also have been used for the Nd:$GdVO_4$ cavities as well.

For the Nd:$GdVO_4$ setups, the reflection losses where rather high within the cavities. The silicone rubber had a refractive index of 1.43, which was not very well matched with the gain medium itself or the in- and outcouplers at $\eta = 2$, 1.517 and 1.49 respectively. Although impossible to match the glue to both the gain medium and the in/outcoupler in this case, some improvements could be done in the matching. One other alternative is of course diffusion bonding instead of the use of glue, which would reduce the reflection losses since there would be two less interfaces and better index matching between the materials.

### 9.2.2 Cavity design improvements

Aside from the possible material improvements, the design itself can also be adjusted to get a better laser performance.

The monolithic cavities (as well as the two trial setups) were made only with Nd:$GdVO_4$, and not Nd:glass. The glass proved to have a too low damage threshold, and the glass medium broke due to the thermal load before lasing. A more efficient cooling system for the gain medium would

reduce this problem, and possibly allow the doped glass to function in a monolithic setup, with such a small pump focus ($40\mu m$). With a highly efficient thermal conductor medium surrounding the cavity, possibly a liquid, perhaps the glass host would be able to deposit the extra heat when pumped despite it's poor thermal properties. Furthermore, pulsed pumping allows higher maximum value before damaging the host material and may enable lasing, even though at very low output powers. For the glass used however, the damage threshold was very low, so threshold may never be reached despite pulsed pump light.

#### 9.2.2.1 Increased beam quality

To get rid of the higher modes, the pump can be focused harder to get a smaller focus in the gain medium, and hence also fewer transversal modes. Although it was quite easy to achieve single longitudinal mode operation for the monolithic laser, it is possible to shorten the gain medium and hence get a shorter cavity resulting in larger longitudinal mode separation. This will probably increase the pump power limit for single mode operation. Also, a shorter gain medium will result in a better overlap of the pump and cavity mode, since the pump was very divergent. To further increase the beam quality of the laser output, a higher quality pump diode could be used. One with lower $M^2$ value results in a smaller focus which may help get rid of higher transverse modes and hence reducing the $M^2$ value of the output. For the setup used, it was hard to decrease the focus size and still be able to place the monolithic cavity so that absorption was maximized (the spacing between the last lens of the pump setup was too close to the incoupler). A lower $M^2$ pump however, would decrease the focus size without having to change the setup.

### 9.2.3 Further development

Further development of the project could be writing the grating directly onto the gain medium. This would decrease the cavity length, as well as removing one interface being a source of reflection loss. This procedure would be simplified having glass as the host material, so a high quality, lasing Nd:glass would be very useful. If one had a working glass material, unfortunately not found in this project, the in/outcoupling mirror curvature could be polished out of the glass itself, further reducing reflection losses. This would lead to a monolithic laser cavity, in it's true sense meaning only one material. Fig.9.1 depicts what such a device could look like. An interesting continuation to the monolithic setup would be frequency conversion. A PPKTP crystal could be used after the outcoupler, but to stay true to the project it would be of more interest to integrate it with the monolithic piece. Doing so, one would attain a monolithic, frequency converted, narrowband monolithic

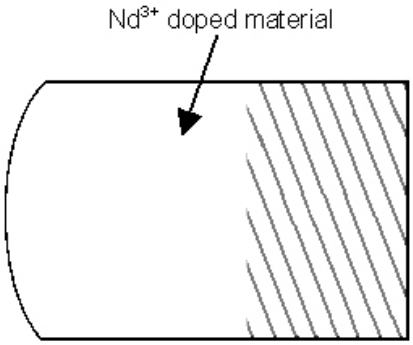


***Figure 9.1.*** *A monolithic laser cavity with a curved side and an internal grating.*

laser. The use of such a setup is of course vast and incites further work and development of the project.

Time limited the experiments to the ones conducted in this project, with a lot of suggestions for future work and further improvements.

# References

[1] RP Photonics, Encyclopedia of Laser Physics and Photonics. http://www.rp-photonics.com

[2] Wikipedia, the free encyclopedia. http://www.wikipedia.com

[3] C. Nordling, J. Österman, *Physics Handbook, 6th ed.* Studentlitteratur, Sweden (2002).

[4] W. T. Silfvast, *Laser Fundamentals, 1st ed.* Cambridge University Press, USA (2000).

[5] E. Hecht, *Optics, 4th ed.* Addison Wesley, San Francisco (2002).

[6] W. Koechner, *Solid-State Laser Engineering, 5th ed.* Springer-Verlag, Berlin (1999).

[7] N. W. Ashcroft, N. D. Mermin, *Solid State Physics.* Thomson Learning Inc., USA (1976).

[8] A. E. Siegman, *Lasers.* University Science Books, USA (1986).

[9] S. Bjurshagen, *Diode-pumped rare-earth-doped quasi-three-level lasers.* Doctoral Thesis in Phys., Royal Inst. of Tech., Stockholm (2005).

[10] C. Czeranowsky, *Resonatorinterne Frequenzverdopplung von diodengepumpten Neodym-Lasern mit hohen Ausgangsleistungen im blauen Spektralbereich.* Doctoral Thesis in Phys., University of Hamburg, Hamburg (2002).

[11] B. Jacobsson, V. Pasiskevicius, F. Laurell, "Single-longitudinal-mode Nd-laser with a Bragg-grating Fabry-Perot cavity." *Opt. Express* **14**, p.9284 (2006).

[12] B. Jacobsson, M. Tiihonen, V. Pasiskevicius, F. Laurell, "Narrowband bulk Bragg grating optical parametric oscillator." *Opt. Lett.* **30**, p.2281 (2005).

[13] H.R. Xia, H.D Jiang, W.Q. Zheng, G.W. Lu, X.L. Meng, H.J. Zhang, X.S. Liu, L. Zhu and J.Y. Wang, "Optical parameters and luminescent properties of Nd:$GdVO_4$." *J. Appl. Phys.* **90**, p.4433 (2001).

[14] B. L. Volodin, S. V. Dolgy, E. D. Melnik, E. Downs, J. Shaw, and V. S. Ban, "Wavelength stabilization and spectrum narrowing of high-power multimode laser diodes and arrays by use of volume Bragg gratings." *Opt. Lett.* **29**, p.1891 (2004).

[15] R. Horváth, L. R. Lindvold, N. B. Larsen, "Fabrication of all-polymer freestanding waveguides." *J. Micromech. Microeng.* **13**, p.419 (2003).

[16] H. Kogelnik, "Coupled wave theory for thick hologram gratings" *Bell Syst. Tech. J.* **48**, p.2909 (1969).

[17] H. Zhang, J. Liu, J. Wang, C. Wang, L. Zhu, Z. Shao, X. Meng, X. Hu, M. Jiang, "Characterization of the laser crystal Nd:$GdVO_4$." *J. Opt. Soc. Am. B* **19**, p.18 (2002).

[18] T. S. Lomheim, L. G. DeShazer, "Optical-absorption intensities of trivalent neodymium in the uniaxial crystal yttrium orthovanadate". *J. Appl. Phys.* **49**, p.5517 (1978).

[19] WinLase software package. http://www.winlase.com